Lactate signalling leads to aggregation of immune-inflammatory hotspots and SLC5A12 blockade promotes their resolution

Michelangelo Certo, Elena Pontarini, Sebastian Gilbert, Ronny Schmidt, Jason Turner, Davide Lucchesi, Daria Apostolo, Giulia Cavallaro, Charlotte Smith, Serena Colafrancesco, et al.

nature metabolism

Article

https://doi.org/10.1038/s42255-025-01331-9

Lactate signalling leads to aggregation of immune-inflammatory hotspots and SLC5A12 blockade promotes their resolution

Received: 7 October 2024

Accepted: 10 June 2025

Published online: 4 August 2025

Check for updates

Michelangelo Certo[1,11] ✉, Elena Pontarini[2,11], Sebastian G. Gilbert[3,9], Ronny Schmidt[4], Jason D. Turner[1], Davide Lucchesi[2], Daria Apostolo[2,5], Giulia Cavallaro[6], Charlotte G. Smith[1], Serena Colafrancesco[7], Joana Campos[1,10], Saba Nayar[1], Christoph Schröder[4], Benjamin A. Fisher[1,8], Fabian Spill[3], Michele Bombardieri[2,12] ✉ & Claudio Mauro[1,12] ✉

Ectopic lymphoid structures (ELS) are aggregates of lymphoid cells that often form within inflamed tissues in patients with autoimmune diseases, cancer, infectious diseases and cardiovascular conditions. These structures drive B cell maturation into memory B cells and plasma cells through B cell and T cell co-stimulation, and their role in pathogenesis is increasingly recognized. Understanding how ELS develop and persist in inflamed tissues is essential for elucidating the pathogenesis and treatment responses in diseases in which they have a prominent role. Here we show that metabolic pathways and specific metabolites, in particular lactate, are master regulators of ELS organization in Sjögren's disease (SjD), the second-most common autoimmune rheumatic disease. Furthermore, inhibiting lactate uptake by lactate transporters, specifically by SLC5A12 blockade, represents a previously unappreciated checkpoint in autoimmune inflammatory diseases. This approach results in multidimensional pro-resolution effects, including reduced inflammatory cytokine levels, enhanced T cell egress from inflamed sites and diminished T cell and B cell areas and their segregation within ELS.

ELS drive B cell maturation into plasma cells through B cell and T cell co-stimulation. Understanding how ELS develop and are maintained in inflamed tissues is crucial, as they impact the progression of infections, autoimmune diseases, cancer, atherosclerosis and transplant rejection[1]. In certain autoimmune conditions, patients with ELS in the inflamed tissue often respond poorly to standard biologics, presenting a substantial challenge therapeutically[1,2]. Conversely, intra-tumoral ELS in solid cancers have been linked to improved clinical responses to immune checkpoint inhibitors[3–5].

Multiple autoimmune diseases, including rheumatoid arthritis, multiple sclerosis and SjD, are characterized by ELS development in target organs. SjD—the second-most common autoimmune rheumatic disease, affecting 0.2–0.5% of the general population—is an excellent model for studying ELS because of the accessibility of labial salivary gland (SG) biopsies and the availability of inducible models of sialadenitis that form ELS[6].

Unlike other inflammatory and autoimmune diseases, in which evidence of ELS influencing disease evolution and treatment response to conventional and biologic treatments is emerging, there is robust evidence that ELS have a pathogenic role in SjD. For example, they are associated with more severe systemic manifestations, including lymphadenopathy and peripheral neuropathy, and a significantly higher risk of progression to B cell MALT lymphoma[1,7–10].

The mechanisms regulating ectopic lymphoid neogenesis in human pathology remain poorly defined. Although these processes involve interactions between immune and non-immune cells specific

A full list of affiliations appears at the end of the paper. ✉e-mail: m.certo@bham.ac.uk; m.bombardieri@qmul.ac.uk; c.mauro@bham.ac.uk

to the local microenvironment where ELS form, they seem to follow stereotypical key steps essential for their development and function across different conditions[2]. Similar to lymphoid organogenesis during embryonic life, lymphotoxin b (LTb) is critically involved in ectopic lymphoid development, leading to the ectopic expression of homoeostatic chemokines such as CXC-chemokine ligand 13 (CXCL13), CC-chemokine ligand 19 (CCL19) and CCL21. This results in increased infiltration of B cells and T cells expressing their specific receptors, CXCR5 (for CXCL13) and CCR7 (for CCL19 and CCL21)[11].

In addition to the classical model of lymphoid neogenesis described above, pro-inflammatory cytokines, particularly those related to early activation of the interleukin (IL)-22–IL-17 pathway and produced by both γδ and conventional CD4 T cells, can also initiate or propagate ELS by inducing lymphoid chemokine production[12–18].

Within the forming ELS, CD4 T cells with B cell helper functions, such as T follicular helper cells (T_{FH}) and the recently described subset of T peripheral helper cells, promote B cell differentiation into germinal centre B cells primarily by the release of the key B cell activating cytokine IL-21 and synergistic co-stimulation through interactions between ICOS–ICOSL and CD154–CD40 (refs. 19–23). Although CD4 T cells have a critical role in ELS formation and function, the signals regulating CD4 T cell responses within the local inflammatory microenvironment of developing ELS remain poorly understood. Recent discoveries highlighting the fundamental role of metabolism in regulating immune cell biology and inflammatory pathways have substantially advanced our understanding of immune cell regulation and related pathologies[24,25].

Studies have recently revealed emerging signalling functions of intermediates and end products of metabolism, such as lactate, acetyl-CoA and succinate, in regulating immunity[26–29]. These metabolites influence cytokine production, interact with transcription factors, modulate ion channel activity and affect cell migration and differentiation[28]. This evolving view suggests that metabolite signalling enables cell-to-cell communication and allows sensing of microenvironmental conditions to trigger stress responses and cellular adaptation[28].

Lactate, traditionally viewed as a by-product of metabolism or a biomarker, has recently been recognized as a multifaceted, bioactive molecule. Lactate accumulation in inflammatory sites significantly impacts tissue-resident and infiltrating immune cells as well as stromal cells. It has been linked to tumour escape from immune surveillance mechanisms through inhibition of macrophage and T cell effector functions[30–34]. At the site of inflammation, accumulation of lactate can lead to metabolic reprogramming, inflammation and angiogenesis[27,28,35,36].

In health, lactate concentrations in blood and tissues are around 1.5–2 mM but can increase to 10–40 mM in inflamed tissues, such as atherosclerotic plaques, adipose tissue in obesity, tumour microenvironments and arthritic joints[37–39]. Elevated lactate levels have been reported in the serum of patients with multiple sclerosis and SjD, with the latter correlating with fatigue and exercise intolerance[36,40]. Lactate is produced in the cytoplasm during hypoxia or as a result of aerobic glycolysis in proliferating cells and is then secreted through the plasma membrane. This transport is mediated by six known solute carrier transporters that perform proton–lactate symport (MCT1–4) or sodium-dependent transport (SMCT1 (SLC5A8) and SMCT2 (SLC5A12)). The transport direction of both systems depends on the lactate gradient, favouring lactate import when extracellular lactate is elevated, such as in inflamed tissues[41,42].

The lactate transporter SLC5A12 is mostly expressed in the distal tubules in the kidney in healthy conditions but has been shown to be upregulated in subsets of CD4 T helper (T_H) cells (T_H1, T_H17, T_{FH}) and B cells within inflamed tissues, but not in the periphery, in autoimmune conditions such as the synovium in rheumatoid arthritis[43,44].

The critical role of CD4 T cells in ELS formation and function has been demonstrated[1,20], and we and others have reported the profound immunoregulatory effects of lactate and its associated transporters on CD4 T cell function, leading to CD4 T cell entrapment in the inflamed tissue and upregulation of key cytokines such as IL-17 and IL-22 (refs. 44,45). We also previously reported that lactate feeding to activated CD4 T cells increases the intracellular pool of acetyl-CoA, initiating a cascade of fatty acid synthesis activation[44]. However, acetyl-CoA can also be used as a substrate for acetylation of various targets, including histones, enzymes and cholesterol or fatty acid synthesis, as well as transcription factors[46].

Given the role of CD4 T cells in regulating ELS formation and function and the importance of lactate in modulating CD4 T cell functions, including migration and IL-17 and IL-22 cytokine outputs, we explored the capacity of lactate and lactate transporters to impact ELS development in the SGs of both animal models and patients with SjD.

Results

Lactate transporter expression associates with metabolism and ELS in SjD

Retrograde cannulation of the submandibular SGs in C57BL/6 mice is an effective method to deliver a replication-deficient adenovirus (AdV)-5, inducing the formation of ELS within the SGs[6]. Following AdV-5 infection, a stepwise infiltration of innate immune cells occurs in the gland, with an early immune response in the SGs during the first 3 days post viral cannulation and activation of key lymphomagenesis pathways by day 5. The initial organization of ELS, characterized by segregated T cell and B cell areas, occurs before day 10, with fully functional ELS development by day 10 onwards (Fig. 1a). SGs were collected at days 0, 5 and 12 post cannulation for longitudinal bulk RNA sequencing (RNA-seq) analysis.

Here, we observed a progressive upregulation of chemokines and chemokine receptors responsible for T cell and B cell recruitment and organization (*Ccl19–Ccr7* and *Cxcl13–Cxcr5*) during ELS formation (from day 5 to day 12) (Fig. 1b and Extended Data Fig. 1a). Additionally, genes associated with the formation of functional ectopic germinal centres were found to be linked to the modulation of lactate metabolism in the SGs, including *Ldha* and *Ldhb*, as well as lactate transporters, as shown in Fig. 1b,c. In the context of germinal centre activity within ELS, T_{FH} cells, defined as $CD4^+$, $CXCR5^+$ and $PD1^+$ T cells

Fig. 1 | Transcriptomic analysis and lactate quantification in SG tissue. **a**, Workflow of the murine sialadenitis model, showing a representation of the mouse submandibular SG and the cannula used for the delivery of the AdV (AV) vector into the gland. The timeline depicts ELS formation within the SGs following injection of the AdV type-5 vector. **b**, Supervised heatmap of differentially expressed genes from bulk RNA-seq of murine SGs collected at 0, 5 and 12 days post cannulation (DPC). **c**, Expression levels of selected genes related to lactate transporters, metabolic enzymes downstream of lactate signalling and inflammatory mediators in murine SGs collected at 0, 5 and 12 days post cannulation ($n = 10$ per time point). Adjusted P values calculated using DESeq2 (*$P < 0.05$, **$P < 0.01$, ***$P < 0.001$, ****$P < 0.0001$). **d**, Lactate concentrations in SGs from non-cannulated (control) and cannulated (experimental) mice at day 5 ($n = 6$ glands per group). Data are expressed as means, normalized to tissue weight; error bars, s.d. Statistical significance was assessed using the Mann–Whitney U-test, **$P < 0.01$. **e**, Schematic overview of the bulk RNA-seq workflow used for analysing human SG tissue. **f**, Expression levels of selected mRNA transcripts related to lactate transporters, metabolic enzymes downstream of lactate signalling and inflammatory mediators in human SGs. This comparison involves sicca and SjD SGs classified as ELS− or ELS+ based on histological analysis of matched biopsies (adjusted P values calculated by DESeq2, *$P < 0.05$, **$P < 0.01$, ***$P < 0.001$, ****$P < 0.0001$). **g**, Scaled average expression and the percentage of cells with any expression of lactate dehydrogenase (LDHA or LDHB) mRNA transcripts per cell cluster in both SjD and non-SjD sicca SGs. Data were generated from disaggregated minor labial SG biopsies ($n = 7$ patients per disease).

https://doi.org/10.1038/s42255-025-01331-9

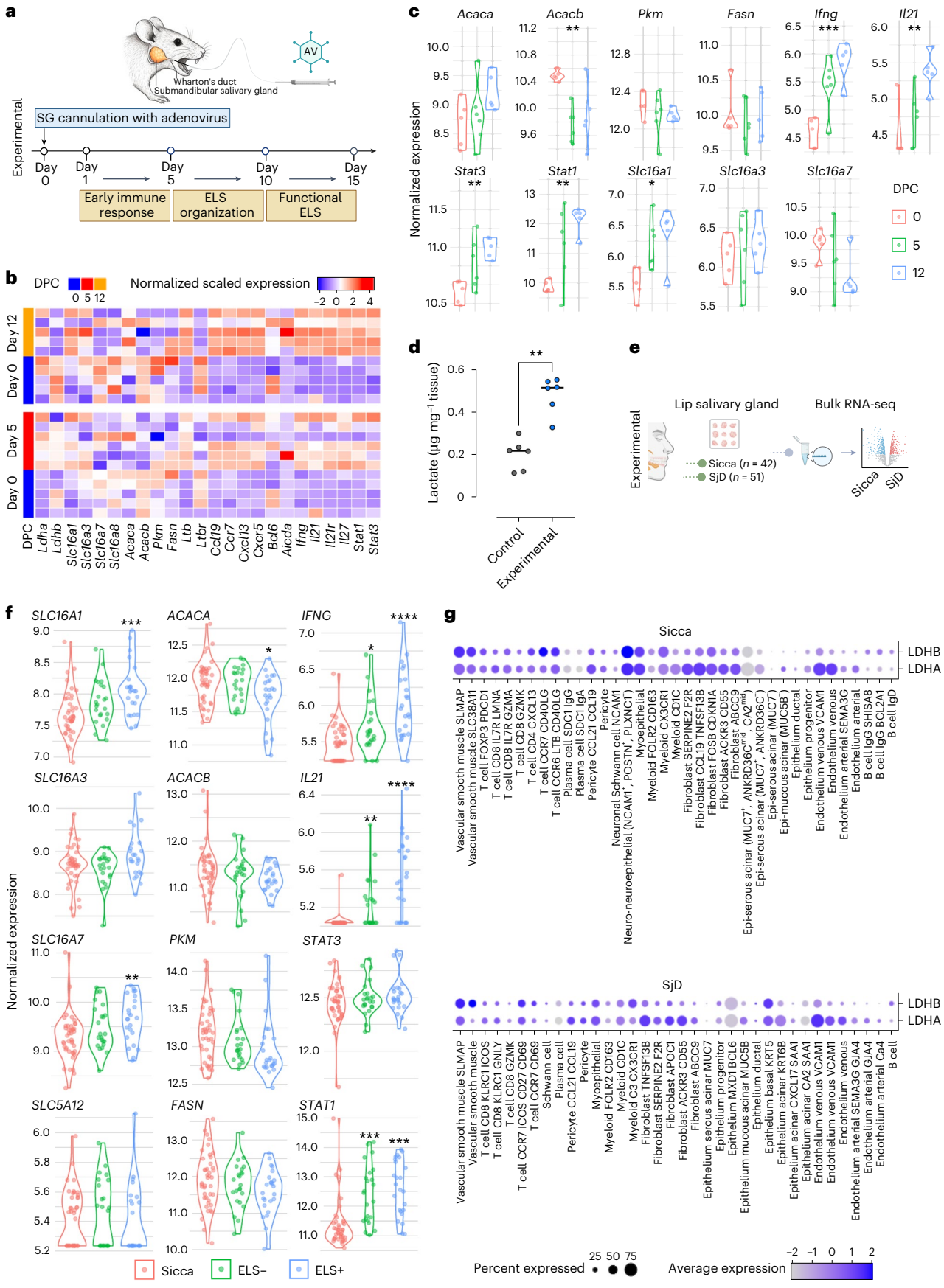

that support germinal centre B cell activation, are the primary source of IL-21 in the mouse SG. T_{FH} cells account for 30% of IL-21-producing $CD4^+$ T cells, and the entire T_{FH} compartment produces IL-21 (Extended Data Fig. 1b).

To further explore the link between lactate metabolism and SG inflammation, we quantified lactate levels in both non-cannulated (control) and cannulated (experimental) mouse SG tissue. A significant increase in lactate concentration was observed in the cannulated group compared to non-cannulated controls (Fig. 1d). These findings reinforce the association between inflammatory processes and altered metabolic states in the SG, as evidenced by the upregulation of lactate transporters and metabolic enzymes linked to lactate in RNA-seq data.

To investigate whether the metabolic changes observed in the viral-induced model of SG ELS could be reproduced in SjD SG, we investigated the associations between the inflammatory response, lactate transporters and metabolic pathways in our bulk SG RNA-seq data from SjD SGs stratified for the presence of ELS (Fig. 1e). The unsupervised clustering of the SG transcriptomic profiles from patients with SjD versus sicca controls (patients with non-autoimmune sialadenitis) revealed a segregation of samples with higher expression of inflammatory mediators known to have a role in organizing inflammatory aggregates into ELS (Extended Data Fig. 1c). ELS-positive samples also showed higher expression of lactate transporters (Fig. 1f and Extended Data Fig. 1c). Inflammatory mediators, such as B cell–T cell chemokine-chemokine receptor axes (CCR7–CCL19, CXCR5–CXCL13) and cytokines (*IFNG*, *IL21*, *IL27*), were progressively upregulated in SjD gland tissue with increasing ELS organization from sparse immune cells (G0) to fully organized ELS (G3) (Fig. 1f and Extended Data Fig. 1c).

Examining lactate transporters from the SLC16 and SLC5A families, alongside metabolic enzymes upstream or downstream of lactate metabolism, we found a clear association between higher lactate transporter expression and ELS organization in SG tissue (Fig. 1f). This association was more pronounced in SjD SGs with ELS compared to SjD SGs without ELS or sicca SGs. Additionally, this was accompanied by the downregulation of metabolic enzymes (*ACACA*, *ACACB*, *PKM* and *FASN*), suggesting reduced usage of fatty acid or cholesterol synthesis from acetyl-CoA derived from lactate, and an increase in inflammatory cytokines (*IFNG* and *IL21*) and mediators (*STAT1* and *STAT3*) in SjD SGs with ELS, compared to SGs lacking this inflammatory feature or sicca controls (Fig. 1f and Extended Data Fig. 1c).

Of note, single-cell RNA-seq data from human SjD and sicca SGs revealed that lactate metabolism is broadly regulated across multiple cell types within the SGs (Fig. 1g). Specifically, we observed widespread expression of lactate dehydrogenase mRNA transcripts, with relatively lower expression in B cells and plasma cells. Notably, higher lactate dehydrogenase expression was detected in $CD8^+$ T cells, fibroblast subtypes and myeloid cells in SjD compared to sicca.

SLC5A12 expression in SjD correlates with key ELS drivers

Given that SLC5A12 expression was relatively low in bulk RNA-seq compared to other lactate transporters (a pattern often observed in publicly available RNA-seq datasets owing to its highly restricted and inducible expression), we further investigated lactate levels as well as SLC5A12 and cytokine expression in SGs from patients with SjD.

We set up SjD SG organ cultures (Fig. 2a) and measured lactate levels in the culture media, finding a correlation with the focus score (a histopathological index of SG inflammatory infiltrate severity that is currently part of the SjD classification criteria[47] and strongly associated with lymphoma progression[48]) of the corresponding lip SG lobule (Fig. 2b). This analysis revealed increased lactate concentrations associated with a higher focus score. Furthermore, egressed cells were analysed by flow cytometry for key T cell cytokine expression (Fig. 2c), and IL-21 levels were quantified in the culture media using ELISA (Fig. 2d).

SjD SG tissue sections were screened for the presence of ELS and classified as ELS-positive or ELS-negative, based on the presence or absence of B cell (CD20) and T cell (CD3) segregation in discrete areas (Fig. 2e). This classification allowed us to specifically target tissues with and without organized immune cell aggregates for comparative analysis. Image analysis of the immunofluorescence staining revealed a significant upregulation of SLC5A12 in CD3 and CD4 T cells within ELS-positive SGs (Fig. 2e,f). To confirm the specificity of the antibody, we performed staining on kidney tissue, a well-established site of high SLC5A12 expression (Extended Data Fig. 1d). The antibody specifically labelled the proximal tubules, where SLC5A12 is predominantly localized, while showing no staining in the distal tubules. This selective staining pattern validates the antibody's specificity in recognizing SLC5A12 within its expected anatomical context.

To ensure that the observed increase in SLC5A12 expression was not merely caused by a higher density of T cells in ELS-positive compared to ELS-negative tissues, we analysed the percentage of CD3 T cells and CD4 T_H cells expressing SLC5A12. The results showed that a significantly higher percentage of CD4 T_H cells expressed SLC5A12 in ELS-positive SGs compared to ELS-negative SGs (Fig. 2f). This finding underscores the preferential upregulation of SLC5A12 in the context of ELS formation.

Moreover, we performed quantitative PCR with reverse transcription to quantify SLC5A12 expression in SG tissues from patients with SjD and sicca controls. Our data demonstrated a positive correlation between SLC5A12 expression and the expression of several genes known to be involved in ELS organization and function (Fig. 2g and Extended Data Fig. 1e). These include CCR7–CCL19 and CXCL13, which are critical for B cell chemoattraction, as well as LTβ, which is crucial for lymphoid tissue organogenesis. Furthermore, we observed a positive correlation with genes involved in germinal centre activity, such as the transcription factor Bcl6 (Fig. 2g and Extended Data Fig. 1e), occurring

Fig. 2 | In vitro SG organ culture and immune cell dynamics in SjD. **a**, Representative images of the in vitro SG organ culture system showing a lip SG lobule from a patient with SjD and the immune cells spontaneously egressing from the tissue. **b**, Correlation plot of the lactate levels measured in the supernatant of the SG organ culture from an SjD patient and the focus score (a histopathological index of SG inflammatory infiltrate severity) of the corresponding lip SG lobule. Spearman correlation coefficient (*r*) and *P* value (two-sided) are shown. **c**, Representative flow cytometry plots showing cytokine production by CD4 T cells egressed from the lip SG in the organ culture system. Cytokine production is shown for T cells obtained from a lip SG with low inflammation (lobule 1, focus score of <1) and severe inflammation (lobule 2, focus score of >1.5). **d**, Detection of IL-21 in the supernatant of SG organ cultures derived from lip ($n = 30$) and parotid ($n = 7$) SGs of patients with SjD. **e**, Representative images of lip SGs from patients with SjD, classified based on the absence (ELS−) or presence (ELS+) of ectopic lymphoid structures. The left columns show B cell (CD20) and T cell (CD3) immune infiltration and their segregation. The middle and right columns depict SLC5A12 expression in all T cells (CD3) and specifically in T_H cells (CD4). Scale bars, 100 µm. **f**, Comparison of cell count (left) and percentages (right) of CD3 T cells and CD4 T_H cells expressing SLC5A12 in ELS− ($n = 6$) and ELS+ ($n = 11$) SGs from patients with SjD. Each dot represents an aggregate. Data are expressed as means, error bars, s.d. Statistical significance was determined using the Mann–Whitney *U*-test between groups ($^*P < 0.05$, $^{**}P < 0.01$). **g**, Correlation matrix of SLC5A12 expression with inflammatory mediator genes relevant for ELS formation and function. Gene expression was evaluated using real-time PCR ($n = 18$). The size of the circles represents the magnitude of each correlation, and the colour indicates the Spearman correlation coefficient (*r*). Statistically significant adjusted *P* values (adjusted for multiple testing with false discovery rate correction) are shown within the dots ($^*P < 0.05$).

https://doi.org/10.1038/s42255-025-01331-9

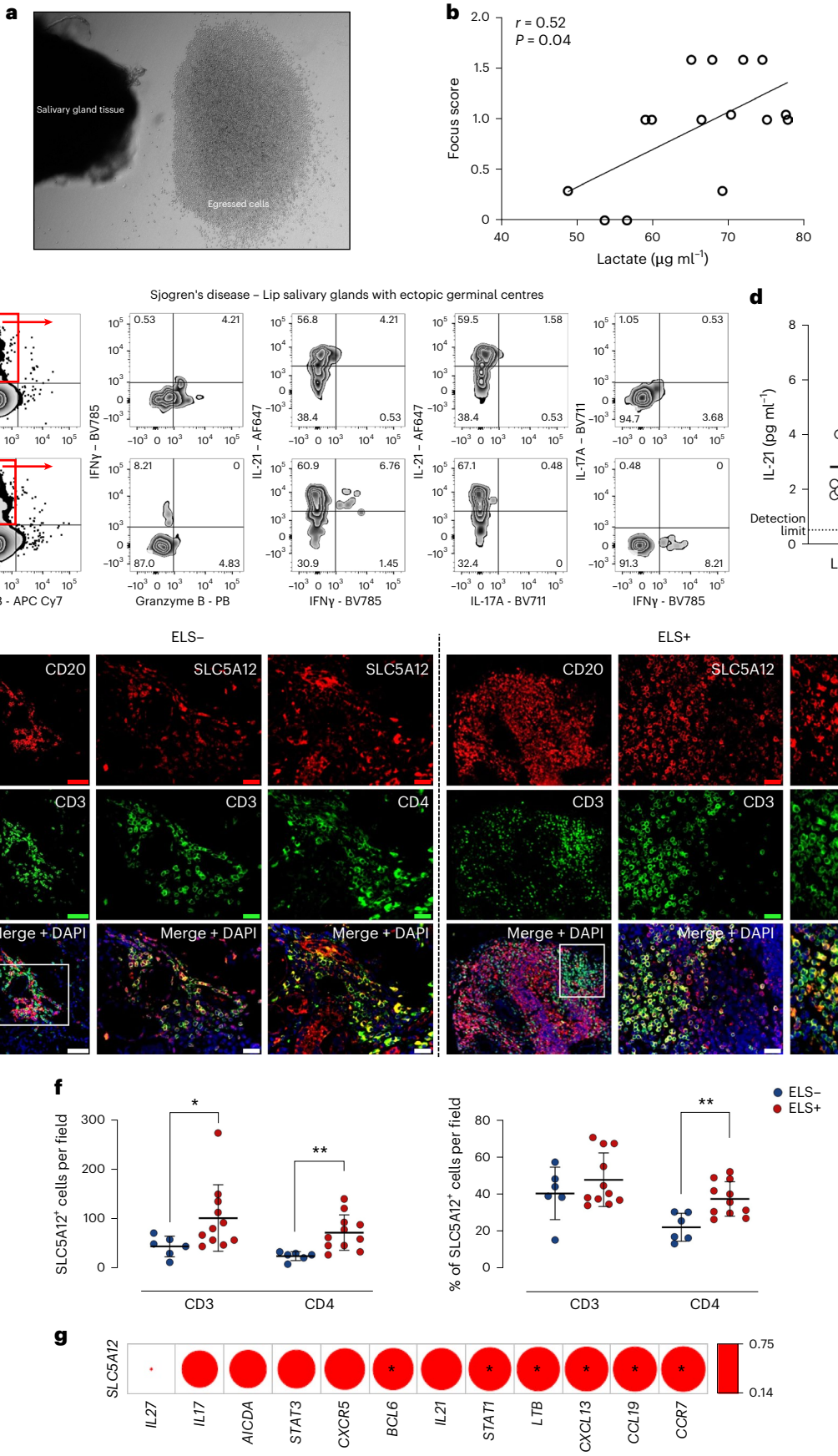

with ELS. These correlations suggest that SLC5A12 might be involved in the metabolic reprogramming of T cells within ELS, potentially contributing to their maintenance and function.

Lactate alters T_H cell profile, boosting IL-21 production

We next assessed whether lactate accumulation influences the autoimmune response, particularly T cell activation and differentiation. To understand how T cells respond in a lactate-rich environment, we activated murine CD4 T cells in the presence of lactate (10 mM) for 12, 24 or 48 h and compared them with CD4 T cells cultured in the absence of lactate. Protein extracts from these cells were subjected to an antibody-based protein array to assess the abundance and acetylation levels of 1,352 proteins (Fig. 3a).

Here, our analysis revealed that approximately 10% of proteins had altered expression after 48 h of lactate stimulation, with 70 proteins upregulated and 43 downregulated (Fig. 3b, Extended Data Fig. 2a–d and Supplementary Data Tables 1–3), suggesting that lactate acts as a master regulator of protein expression in activated CD4 T cells under in vitro conditions, mimicking inflamed tissue. Notably, several inflammatory factors were affected, with IL-17, IL-21 and IL-22 levels being upregulated, and alterations observed in acetylation levels for IL-6RA, STAT1 and IL-1B (reduced) and TSP1 (increased) (Fig. 3c, Extended Data Fig. 3a–c and Supplementary Data Tables 4 and 5).

Additionally, STAT1 acetylation was reduced at 12 and 24 h of lactate treatment but increased again at the 48 h time point, concomitantly with increased abundance (Fig. 3d). Correspondingly, IL-21 abundance increased during periods of STAT1 deacetylation and decreased once STAT1 acetylation was restored (Fig. 3e). IL-21 is known to regulate STAT3, and consistent with IL-21 upregulation at 24 h, we observed increased phosphorylation of STAT3 (Fig. 3f).

KEGG pathway analysis identified T_H17 (IL-17/IL-22) and T_H1 and T_H2 pathways as the main pathways activated by lactate treatment in CD4 T cells activated in vitro (Fig. 3g). This suggests that lactate not only influences protein expression and acetylation but also modulates key inflammatory pathways in T_H cells, promoting a T_H17/T_H1 response and highlighting its potential role in autoimmune responses.

B cell depletion in SjD alters SG ELS with lactate and enzyme modulation

We recently demonstrated that immunomodulating agents, such as the B cell depleting agent (monoclonal anti-CD20 antibody, rituximab), effectively prevented or reduced ELS formation within SjD SGs compared to the placebo-treated group[49].

Hence, we next investigated whether modulation of inflammation in SjD SGs through rituximab was linked to changes in lactate transporters and metabolic enzymes. To address this question, we analysed data from the TRACTISS randomized clinical trial in SjD, which provides comprehensive longitudinal transcriptomic data on SG tissue (Fig. 4a).

Importantly, decreased recruitment of B cells, diminished T_{FH} cell differentiation and lower levels of IL-21 were accompanied by a progressive downregulation of lactate transporters and related metabolic enzymes over time (Fig. 4b), indicating a shift in the metabolic needs of the SG tissue in response to immunomodulatory therapy affecting ELS organization and function.

Lactate sustains IL-21 in SjD, reversed by SLC5A12 mAb blockade

Given the close association between IL-21, lactate transporters and metabolic changes that we observed in SjD SG with ELS, we next evaluated the effect of lactate on IL-21 expression in peripheral blood mononuclear cells (PBMCs) isolated from patients with SjD who had biopsies positive for ELS (Fig. 5a). These patients were selected because of their high circulating levels of IL-21, which we recently showed to be associated with a higher frequency of circulating T_{FH} cells displaying aberrant IL-21 secretion[20].

Lactate stimulation led to a significant increase in IL-21 secretion in PBMCs from patients with SjD, surpassing the high levels they expressed basally, while no such effect was observed in cells from healthy controls (Fig. 5b). Furthermore, blocking SLC5A12 with the specific monoclonal antibody (mAb) 3C7 reduced IL-21 production compared to the isotype control, and this effect was again noted exclusively in PBMCs from patients with SjD (Fig. 5c), highlighting the potential specificity of SLC5A12 blockade.

Overall, these data suggest that lactate promotes or sustains elevated IL-21 production by CD4 T cells, which are primarily T_{FH} cells in SjD. The findings indicate that lactate might contribute to the pathophysiology of SjD by enhancing the inflammatory response mediated by T follicular cells.

SLC5A12 blockade impacts ELS in an inducible Sjögren's model

We next evaluated the formation and function of inflammatory infiltrates and ELS through the genetic or pharmacological blockade of SLC5A12 in the viral-induced murine model of sialadenitis, which mimics focal lymphocytic aggregation and ELS in SjD (Figs. 6a and 7a). Deletion of *Slc5a12* in mice led to significant reduction in inflammatory aggregates (Fig. 6b and Extended Data Fig. 4a,b) as demonstrated by a reduced SG focus score (Fig. 6c) and aggregate area fraction (Fig. 6d), both of which are used as histopathological indexes of SG inflammatory infiltrate severity in clinical practice[50]. We also observed clear alterations in ELS formation (Fig. 6e), characterized by a reduced T cell area, a trend toward a reduced B cell area and decreased B cell–T cell intersection, indicating the extent of B cell–T cell interactions (Fig. 6f), as assessed by an automated image analysis software we developed. Furthermore, we observed a decreased B cell–T cell segregation (Fig. 6g). RT–qPCR analysis of SG tissues showed impacts on *Ltb* and *Ltbr*, as well as *Il21* and *Il21r*, with trends indicating a reduction in various inflammatory genes associated with ELS, including chemokines and chemokine receptors (Fig. 6h). Interestingly, in this model, which is not IL-17-dependent owing to the strong restriction of IL-17 expression by myeloid-cell derived IL-27 (ref. 12), the deletion of *Slc5a12* did not significantly affect *Il17* expression (Fig. 6h).

Similarly, pharmacological blockade of SLC5A12 with the 3C7 mAb, administered therapeutically in two doses on days 4 and 10 of the inducible SjD model (Fig. 7a), had a profound impact on inflammatory aggregates (Fig. 7b and Extended Data Fig. 5a,b) as demonstrated by a

Fig. 3 | Acetylation study of murine CD4 T cells. a, Experimental workflow for the acetylation study of murine CD4 T cells. Lymph nodes and spleen were collected from mice and processed to obtain a single-cell suspension, from which CD4 T cells were isolated. The isolated CD4 T cells were then activated with CD3 and CD28 and treated with lactate or left untreated for 12, 24 and 48 h. The cells were then used to perform a protein acetylation array to assess abundance and levels of acetylation. **b**, Bar graph listing the number of antibodies with differential intensities when comparing untreated versus lactate-treated (12 h, 24 h and 48 h) CD4 T cells. For each comparison, red indicates upregulated proteins, while blue indicates downregulated proteins. **c**, Overview of differences in protein abundance and acetylation levels between untreated and lactate-treated (24 h) CD4 T cells. FC, fold change. **d**, Overview of differences in STAT1 abundance and acetylation levels between untreated and lactate-treated (12 h, 24 h and 48 h) CD4 T cells. **e**, Relative IL-21 levels in untreated and lactate-treated (12 h, 24 h and 48 h) CD4 T cells. For analysis of the samples, a one-factorial linear model was fitted with LIMMA, resulting in a two-sided *t*-test (*$P < 0.05$). Each sample was measured by four replicate spots per array ($n = 3$ biological replicates). **f**, Western blot analysis showing the levels of pStat3 and total Stat3 in CD4 T cells. The cells were either left untreated or treated with lactate for 24 h. Data are presented as mean values; error bars, s.d. Statistical significance was assessed using the Mann–Whitney *U*-test (*$P < 0.05$, $n = 6$ biological replicates). **g**, Selected KEGG pathways related to proteins with differential abundance and acetylation in untreated versus lactate-treated (24 h) CD4 T cells.

https://doi.org/10.1038/s42255-025-01331-9

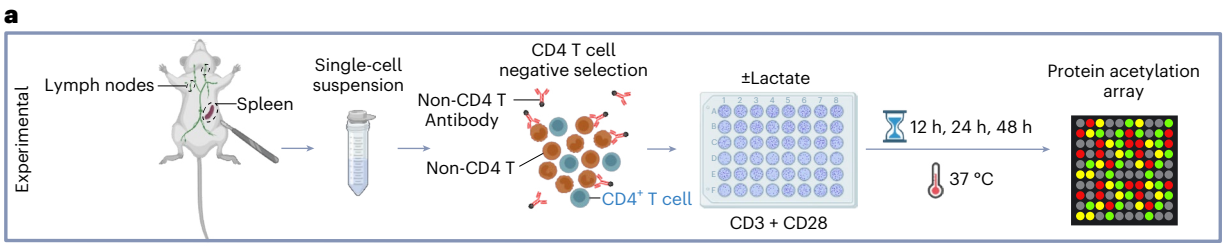

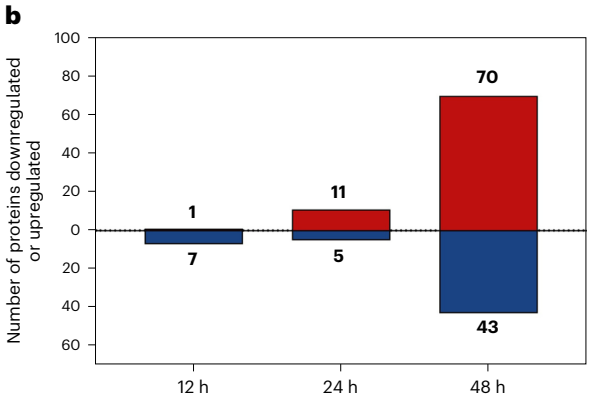

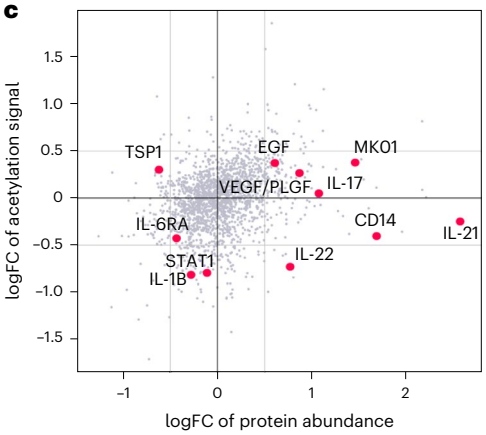

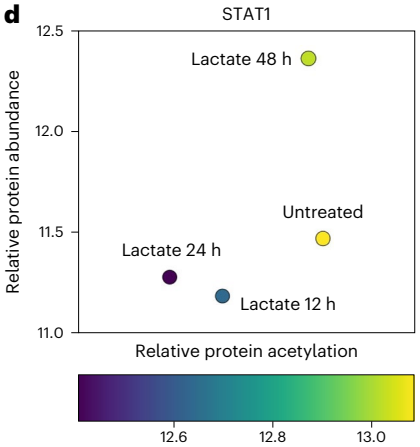

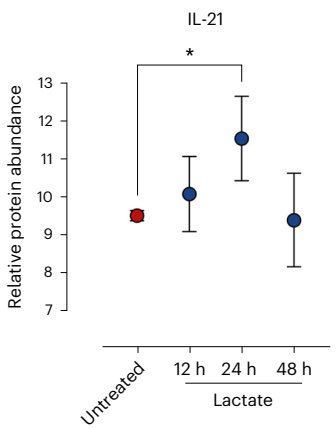

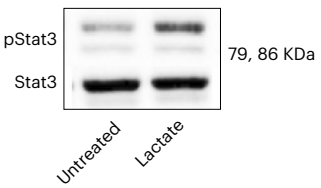

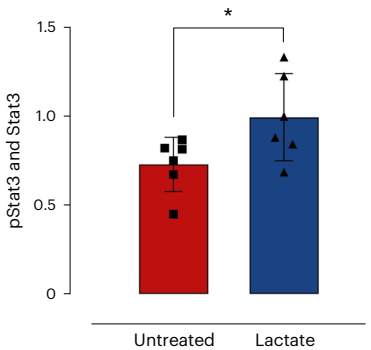

g

Pathway description	Proteins
T_H17 cell differentiation	IFNγ, IL-17A, IL-2, IL-22, IL-6, IL-6R, IRF4, JAK3, NFKBIA, STAT1
Jak–STAT signaling pathway	CCND2, IFNγ, IL-12A, IL-13, IL-2, IL-22, IL-6, IL-6R, JAK3, STAT1
T_H1 and T_H2 cell differentiation	IFNγ, IL-12A, IL-13, IL-2, JAK3, NFKBIA, STAT1
IL-17 signaling pathway	CCL7, IFNγ, IL-13, IL-17A, IL-6, NFKBIA, S100A9

https://doi.org/10.1038/s42255-025-01331-9

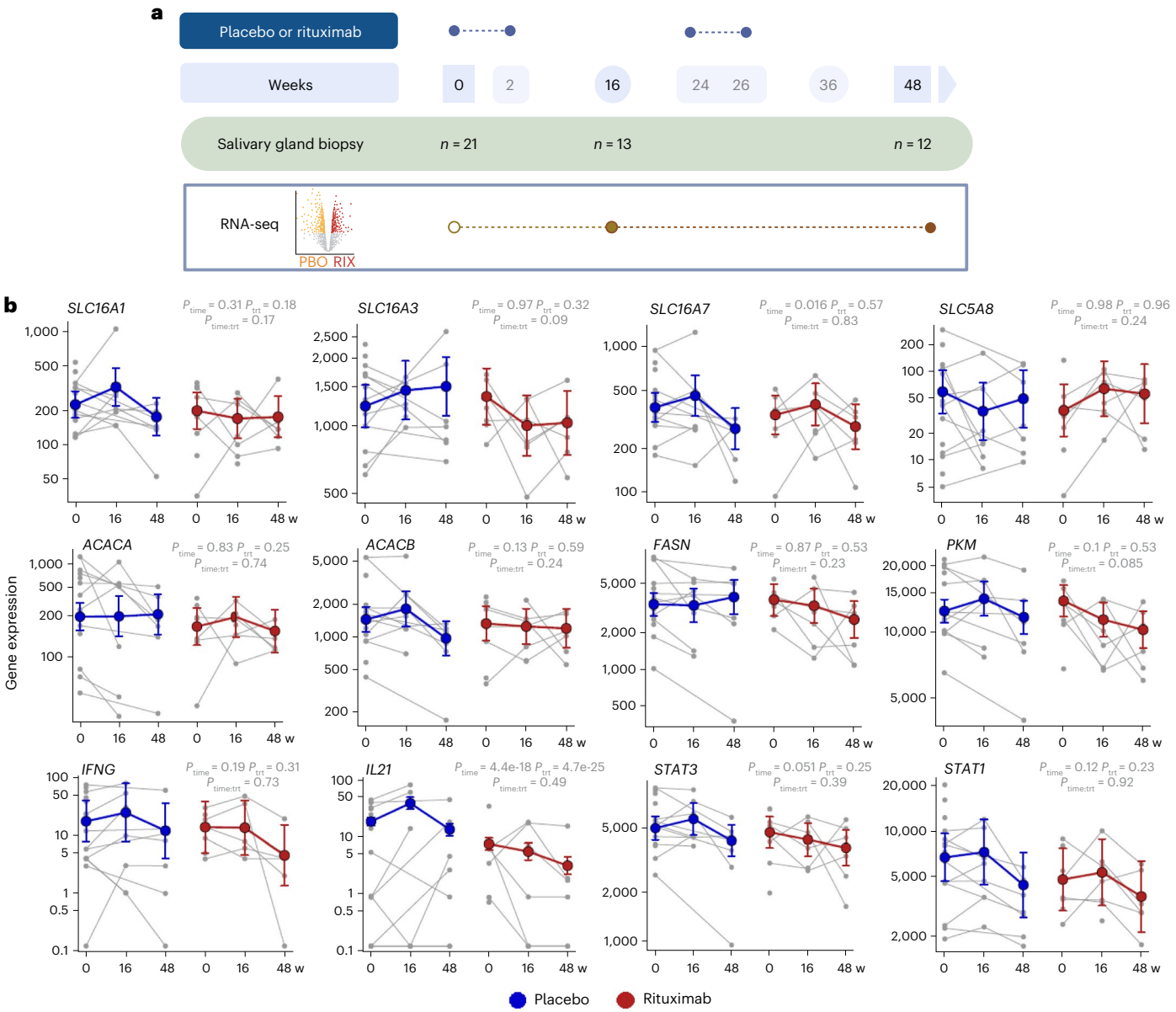

Fig. 4 | Longitudinal transcriptomic profiling of SG tissue in the TRACTISS trial. a, Schematic of the longitudinal transcriptomic study from the TRACTISS randomized clinical trial in patients with SjD, including sequential lip biopsies from patients randomized to either placebo (PBO) or rituximab (RIX) (anti-CD20 B cell depleting agent) treatment. **b**, Changes over time in the expression of genes for lactate transporters, metabolic enzymes downstream of lactate signalling and inflammatory mediators. Blue (placebo) and red (rituximab) lines represent the fitted negative binomial mixed-effects model with a 95% confidence interval. The *P* values of the week/treatment ratio interaction model are shown on top. Data from patients with SjD treated with placebo ($n = 12$) or rituximab ($n = 8$) are included.

reduced SG focus score (Fig. 7c) and aggregate area fraction (Fig. 7d). This treatment led to alterations in ELS formation (Fig. 7e), characterized by decreased areas occupied by both T cells and B cells, reduced B cell–T cell intersection area (Fig. 7f) and decreased B cell–T cell segregation (Fig. 7g). Again, RT–qPCR of SG tissues from ELS areas showed impacts on *Ltb*, *Ltbr*, *Il21*, *Il21r* and *Cxcl13*, with trends towards a reduction in various inflammatory genes associated with ELS, including other chemokines and chemokine receptors (Fig. 7h). Consistent with the genetic model, blocking *Slc5a12* did not significantly impact *Il17* expression (Fig. 7h), reinforcing the selectivity of SLC5A12 targeting.

Overall, these data demonstrate that lactate accumulation in the local SG microenvironment functionally regulates ELS development and function through sensing by lactate transporters on immune cells, primarily infiltrating CD4 T cells. The functional impact of lactate and its transporters on T_H subsets is particularly evident for IL-21 modulation, a key cytokine involved in germinal centre formation and B cell differentiation. These findings highlight the critical role of lactate in sustaining the inflammatory environment in SjD that favours ELS development and suggest that targeting the lactate transporter SLC5A12 could be a promising therapeutic strategy for resolving ELS.

Discussion

Lactate build-up has been observed in numerous disease microenvironments, ranging from inflamed tissues in autoimmune and cardiovascular diseases to tumour microenvironments, infected lungs and obese abdominal adipose tissue[37]. Chronic lactate accumulation at these sites is associated with disease progression; however, the mechanisms induced by lactate may be context-dependent. In cancer, lactate has been linked to the promotion of immune suppression, including the induction of regulatory T cells[34] and anti-inflammatory macrophages,

https://doi.org/10.1038/s42255-025-01331-9

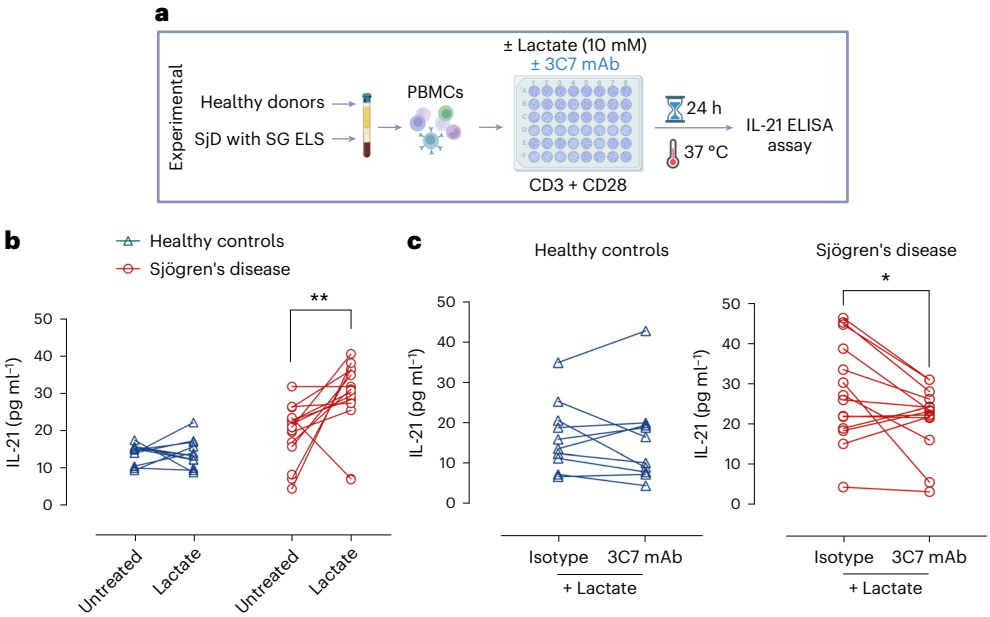

Fig. 5 | Quantification of IL-21 in ex vivo PBMCs from patients with SjD. **a**, Schematic representation of the IL-21 quantification workflow from ex vivo supernatant. **b**, Levels of IL-21 in culture supernatant of PBMCs from patients with SjD with SG ELS ($n = 15$) and from healthy donors ($n = 12$), stimulated in the absence and presence of lactate (10 mM). Lines connect dots representing PBMC samples treated with lactate or left untreated from the same donor. Statistical analysis was performed using the Wilcoxon signed-rank test (*$P < 0.05$, **$P < 0.01$). **c**, Levels of IL-21 in culture supernatant of PBMCs from patients with SjD, stimulated with lactate (10 mM) and treated with either anti-SLC5A12 3C7 mAb or its isotype control. Lines connect dots representing PBMC samples treated with anti-SLC5A12 mAb and its isotype control from the same donor. Statistical analysis was performed using the Wilcoxon signed-rank test; *P* value (two-sided) is shown (*$P < 0.05$).

fostering an environment permissive to further tumour growth[51]. However, in autoimmune tissues, such as rheumatoid arthritis, lactate produced by synovial fibroblasts is taken up by infiltrating CD4 T cells[44] or γδ T17 cells[45]. This uptake leads to increased production of IL-17 by T_H cells, which further promotes the inflammatory autoimmune process[44,45]. Similarly, SG epithelial cells from patients with SjD, targets of autoimmune reactions and active participants in sustaining inflammation, showed increased expression of glucose transporter-1 (GLUT-1) upon activation, suggesting a metabolic shift towards glycolysis, where lactate is the main end product[52].

ELS have been identified in the microenvironments of various diseases, including autoimmune disorders, cancer, cardiovascular conditions and infectious diseases[53]. These aggregates of B cells and T cells possess specialized functions, including the production of autoantibodies, inflammatory cytokines and chemokines, which contribute to the disease process[1]. The main drivers of ELS formation are LTb and LTbr[54]. Additionally, chemokines, chemokine receptors and inflammatory cytokines have been implicated in ELS formation and maintenance[54]. Whether metabolic processes are involved in the organization or function of ELS is currently unknown. We and others have shown that lactate promotes the entrapment of immune cells at sites of inflammation and metabolic reprogramming, leading to increased IL-17 production[44]. Both signals are potentially important in the steps of ELS organization. Hence, we reasoned that lactate could serve as a master regulator of ELS formation in inflamed tissues.

Indeed, our study shows that lactate transporters are preferentially upregulated in the SG of SjD with ELS, associating with the modulation of metabolic and inflammatory genes, particularly *IL21* and *STAT1*. These genes are involved in the signals of ELS organization in SjD SGs[49], as seen in human biopsies from the largest UK cohort of patients with SjD and the TRACTISS trial, critically linking lactate and lactate transporters to disease severity in SjD.

The lactate levels in autoimmune-inflamed tissues, such as the SG in SjD or the synovial joint in rheumatoid arthritis, typically range between 10 mM and 15 mM, compared to 1–2 mM in the blood of healthy individuals. This increase in lactate contributes to a lower pH in the inflamed tissue, although it generally does not fall below pH 6.9. Given that the pKa of lactate is 3.83, very little lactic acid will be present in the tissue, with sodium lactate being the predominant form. Therefore, lactate-H^+ transporters like MCT1 and MCT4 are not likely to have a substantial role in this context, whereas a Na^+-lactate transporter such as SLC5A12 is likely to be more relevant. By contrast, in the tumour microenvironment, lactate concentrations can reach up to 40 mM, resulting in a more pronounced pH drop (down to around pH 6), which may enhance the relevance of lactate-H^+ symporters. Furthermore, although MCT1 and MCT4 are expressed in most tissues and are highly expressed under steady-state conditions, SLC5A12 expression is normally restricted to the proximal tubules of the kidney, small colon and retina[55]. In the context of inflammation, however, SLC5A12 is upregulated in specific immune cell subsets, such as $CD4^+$ T_H17, T_{FH} and B cells, and is only expressed within the diseased tissue. Previous studies have demonstrated that blockade of SLC5A12 can have functional and disease-improving effects[27,43,44]. Conversely, SLC5A12 expression in $CD8^+$ T cells is minimal, and its blockade does not appear to affect macrophage function.

Given that this upregulation is tissue-specific and not observed in peripheral tissues[44], we believe targeting SLC5A12 could yield therapeutic benefits while minimizing side effects, in contrast to the adverse outcomes observed in clinical trials targeting MCT1.

ELS have been reported in cancer, where they have been associated with clinical response to PD1 immune checkpoint blockade[47]. However, to the best of our knowledge, no current evidence links metabolic reprogramming to the formation of ELS in cancer, and it is possible that such drivers are specific to the tumour microenvironment.

Furthermore, we reveal that lactate acts as a master regulator of the expression of about 10% of the investigated proteome of activated CD4 T cells in conditions mimicking the build-up of lactate

in the inflamed tissue and modifies the acetylation levels of several targets. One important pathway regulated by lactate is the STAT–IL-21 axis. Lactate induces IL-21 production in PBMCs from patients who are ELS-positive, and blocking SLC5A12 with a mAb (3C7) that we have generated and are developing for therapy results in reduced levels of IL-21.

Together with the reduction of IL-21 and induction of ELS resolution, we have previously shown egress of immune cells from the inflamed site and reduction of IL-17. Therefore, SLC5A12 blockade shows multidimensional beneficial effects which are reminiscent of blockade of PD1 and CTLA4 in immuno-oncology, leading us to propose that SLC5A12 represents an important example of a checkpoint in inflamed tissues in autoimmune diseases.

Being solely expressed at high levels in the diseased tissue[44], SLC5A12 also represents an ideal target to avoid widespread immune suppression and unnecessary targeting of peripheral immune cells. We tested whether targeting SLC5A12 genetically or pharmacologically would modulate ELS aggregation in a viral-induced inducible murine model of ELS within the SGs mimicking SjD[6]. Strikingly, both approaches led to a significant reduction of ELS aggregation, with downregulation of both effects, particularly on LTb and IL-21 pathways, suggesting a role for lactate both in the formation and function of ELS. We previously showed that in this model, ELS formation is independent of IL-17 (ref. 14) because of restriction of IL-17 expression by IL-27 (ref. 12). Hence, the evidence that SLC5A12 blockade has no effect on healthy donors or on IL-17 outputs in the murine model of SjD is particularly important, as it suggests that targeting SLC5A12 results in beneficial immunomodulatory effects dependent on the local inflammatory microenvironment. Additionally, evidence that lactate and SLC5A12 blockade selectively modulate activated CD4 T_H cells in SjD but not in healthy donors demonstrates selectivity of action, which might reduce off-target detrimental effects, such as compromising T_H17 immunity required for skin and gut homeostasis.

Overall, our data demonstrate a previously unrecognized metabolic control of ELS organization, showing that the metabolite lactate acts as a master regulator of ELS formation through modulation of tissue-specific CD4 T cell functions (Extended Data Fig. 6). Additionally, our findings suggest that the inducible SLC5A12 lactate transporter represents an important checkpoint in autoimmunity, whereby both gene targeting and pharmacological blockade plastically modulate key inflammatory pathways that are specific to the local microenvironment in which ELS develop. Hence, therapeutic interventions with the capacity to interfere with lactate-driven immunopathology may impact not only autoimmune diseases such as SjD but also other conditions in which ELS exert a key role in orchestrating disease-specific local immune responses, including cancer, infection and graft rejection.

Methods

Human samples

The current study includes two distinct SjD cohorts: an observational disease–control cohort (SjD–sicca) and the TRACTISS randomized clinical trial, comparing rituximab versus placebo treatment in patients with SjD (Supplementary Data Table 6).

The human study, including the disease–control cohort (SjD–sicca), was approved by the Research Ethics Committee (reference 17/WS/0172), West of Scotland REC 4 and the Research Ethics Committee (reference 05/Q0702/1), NRES Committee London–Westminster. All patients provided written consent according to the principles of the Declaration of Helsinki. Labial SG biopsies were collected after informed consent from patients displaying xerostomia and xerophthalmia and meeting the 2016 American–European Consensus Group (AECG) criteria for SjD[47], alongside patients with non-specific chronic sialadenitis (sicca, controls).

The TRACTISS randomized clinical trial was approved by the Leeds Research Ethics Committee (10/H1307/99). A cohort of patients with SjD ($n = 133$) received either two doses, 2 weeks apart, of intravenous rituximab (1,000 mg) or placebo (250 ml saline) in two courses at weeks 0, 2 and 24, 26, in combination with corticosteroid in both arms. A subset of the patients with SjD part of the TRACTISS study ($n = 29$) consented for a lip biopsy at weeks 0, 16 and 48, providing written informed consent[47].

Animal experiments

The study was approved by the institutional Animal Welfare and Ethical Review Body (UoB PPL PP1011240 and QMUL PPL P29EDC088, Home Office). Young adult male C57BL/6 mice (Charles River Laboratories) and *Slc5a12* knockout mice (produced at the Sanger Institute by CRISPR–Cas9), aged between 10 and 13 weeks at the start of the experiments, were housed in a specific-pathogen-free animal facility under standard conditions. Animals were maintained in ventilated cages with a 12 h light–dark cycle, at a constant temperature of 22 ± 2 °C and relative humidity of 50 ± 10%. Mice had ad libitum access to food and water. Environmental enrichments were added to all cages. Genotyping of ear notches taken at weaning was performed by Transnetyx. Mice were randomly assigned to experimental groups, ensuring that the age and weight were matched between groups. Mice were anaesthetized with ketamine (60 mg kg^{-1}) and xylazine (12 mg kg^{-1}) administered intraperitoneally. Analgesia was provided as 0.1 mg kg^{-1} buprenorphine hydrochloride by subcutaneous injection. The submandibular gland was cannulated through the excretory duct using heat-drawn glass gas chromatography tubing (0.1 mm internal diameter; Sigma-Aldrich). Approximately 20 µl of AdV solution, equivalent to 1×10^8 plaque-forming units of reporter-encoding AdV or buffer vehicle, was injected into the submandibular gland using an attached

Fig. 6 | Histological analysis, immune characterization and gene expression quantification in wild-type and *Slc5a12* KO murine SGs. a, Workflow of the cannulation of murine SGs in wild-type (WT) and *Slc5a12* knockout (KO) mice model showing a representation of the mouse SG, and the cannula used for precise delivery of the AV into the gland. The experimental timeline shows that the AV was injected into the SG on day 0, and on day 14, SG tissues were collected for subsequent analyses. Post collection, tissues were processed for immunofluorescence and qPCR to assess relevant biomarkers and gene expression levels. **b**, Representative images of hematoxylin and eosin (H&E) staining of the whole SGs from WT and *Slc5a12* KO mice. Black arrows point to inflammatory foci (peri-ductal leukocytic infiltrates with more than 50 lymphocytes). **c**, Comparison between WT and *Slc5a12* KO mice ($n = 5$ per group) of focus score calculated on H&E images. **d**, Aggregate area fraction (% of SG area occupied by the inflammatory infiltrate), measured on immunofluorescence stainings. **e**, Representative immunofluorescence staining of SG tissue sections from WT and *Slc5a12* KO mice. CD3 (green) is used as a marker for T cells, B220 (red) is used as a marker for B cells and DAPI (blue) is used as a marker for nuclei. The images reveal the distribution and localization of T cell and B cell inflammatory aggregates in the tissue. Scale bars, 100 µm. **f**, Comparison between WT and *Slc5a12* KO mice of positive area for CD3 (T cells), B220 (B cells) and both (T cell–B cell intersection), respectively, as calculated from **e**. Data are presented as means; error bars, s.d. ($n = 4$ biological replicates per group). Statistical analysis was performed using an unpaired *t*-test. In **c**, **d** and **f**, box and whisker plots show the 75th and 25th percentiles of the data, and minimum and maximum values. Statistical significance was determined using a Mann–Whitney *U*-test (two-sided). **g**, Prevalence of segregated and non-segregated aggregates over the total number in WT and *Slc5a12* KO mice, as calculated from **e**. **h**, qPCR analysis of gene expression levels for *Cxcr5, Cxcl13, Ccr7, Ccl19, Ltb, Ltbr, Il17, Il21* and *Il21r* in WT and *Slc5a12* KO mice. Gene expression levels are normalized to a housekeeping gene and presented as relative expression levels. Data are expressed as means from $n = 8$–10 mice per group; error bars, s.d. Statistical significance was determined using a Mann–Whitney *U*-test (two-sided) and outliers were excluded by Grubb's test (*$P < 0.05$, **$P < 0.01$, ***$P < 0.001$, ****$P < 0.0001$).

https://doi.org/10.1038/s42255-025-01331-9

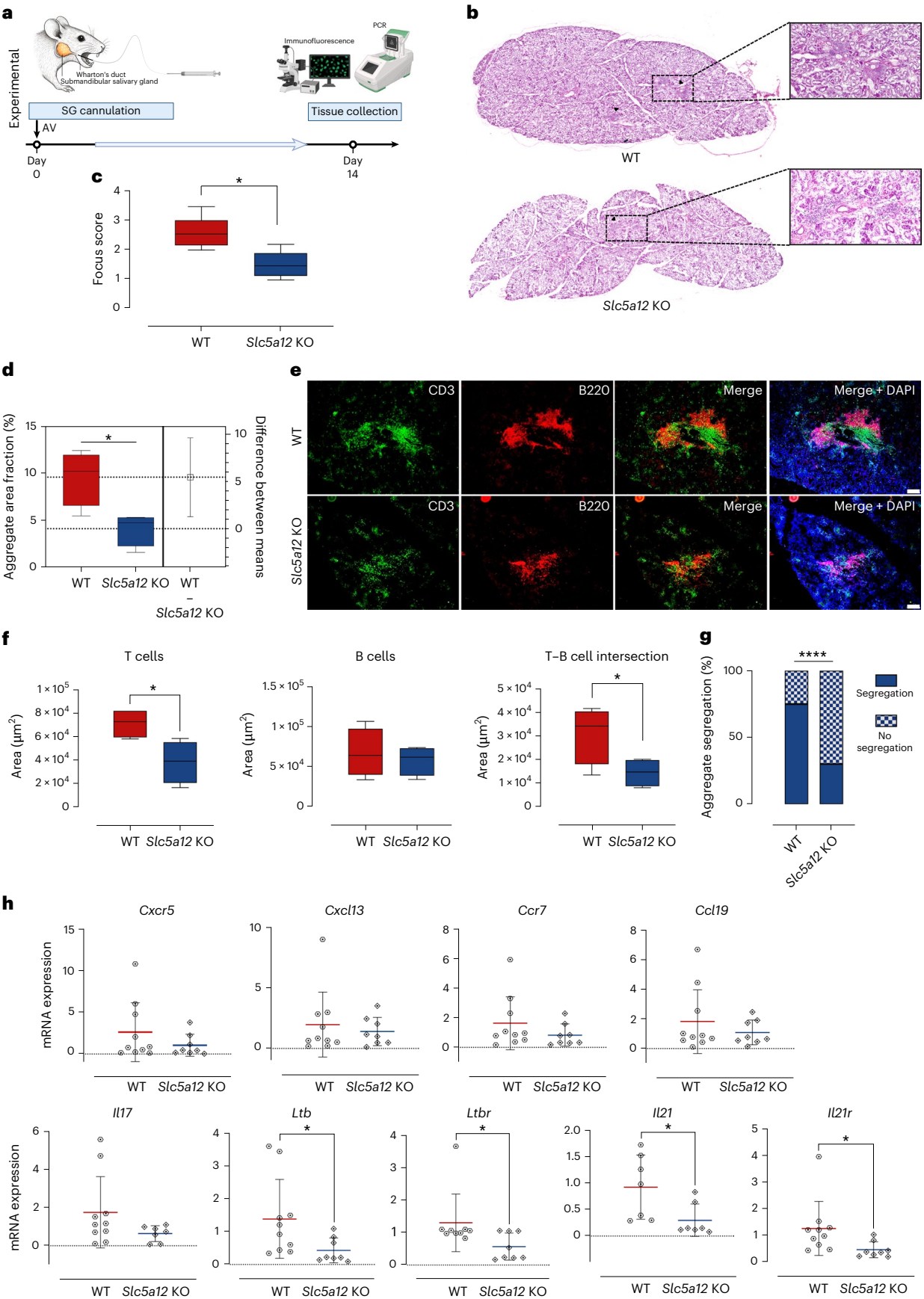

Hamilton syringe (Sigma-Aldrich). The same volume of the vehicle buffer was delivered as a negative control. In the treated group, 3C7 mAb was injected into the gland on days 4 and 10. Mice were killed under terminal anaesthesia on day 14 post cannulation. The submandibular glands were removed, with tissues partly snap-frozen in OCT (Sakura Finetek) for cryosectioning and partly stored in RNAlater (Ambion) for gene expression profiling.

Bulk RNA-seq transcriptomics

RNA samples obtained from murine submandibular SGs were stored in RNAlater solution immediately after collection. Total RNA was extracted using the Qiagen RNeasy Mini Kit (Qiagen) according to the manufacturer's instructions. RNA concentrations and purity were measured using a Qubit 2.0 Fluorometer (Invitrogen), and RNA integrity was assessed using the TapeStation system (Agilent Technologies). For each sample, 500 ng of total RNA was outsourced for bulk mRNA sequencing.

RNA samples were also obtained from labial SG lobules of patients with SjD, sourced from two distinct cohorts: an observational disease–control cohort consisting of patients with SjD and those with sicca as controls, and the TRACTISS randomized clinical trial, which compared rituximab to placebo with longitudinal data collected before and after treatment. Detailed patient information for the SG transcriptomic analysis cohorts is available[49].

Labial SG biopsies were stored in RNAlater solution (Thermo Fisher Scientific) immediately following collection. Total RNA was extracted using the RNeasy Micro Kit (Qiagen) according to the manufacturer's instructions. RNA concentrations and purity were quantified using a Qubit 2.0 Fluorometer (Invitrogen), and RNA integrity was assessed using the TapeStation system (Agilent Technologies). For each sample, 500 ng of total RNA was outsourced for bulk mRNA sequencing.

RNA-seq data were analysed using R (v.4.2.1) within the RStudio environment (v1.2.5042). Differentially expressed genes were identified using the DESeq2 package (v.4.2.1), comparing expression between the sicca and SjD groups, between placebo and rituximab groups in the TRACTISS trial cohort or between murine RNA-seq time points (0, 5 and 12 days post cannulation). The analysis focused solely on protein-coding genes. Gene expression levels were normalized using the variance stabilizing transformation method, and heatmaps were generated using the ComplexHeatmap package (v.2.6.2).

Single-cell RNA-seq transcriptomics

Single-cell RNA-seq data generated from minor labial SG biopsies from patients with SjD or non-Sjögren's sicca were accessed from the Gene Expression Omnibus database under accession code GSE272409. Data were analysed using R (v.4.4.0) and Seurat (v.5.1.0).

qPCR analysis

Total RNA was extracted from the samples using the RNeasy Mini Kit (Qiagen) following the manufacturer's protocol. The concentration and purity of the extracted RNA were assessed using a NanoDrop spectrophotometer (Thermo Fisher Scientific). Subsequently, 1 µg of RNA was retrotranscribed to complementary DNA (cDNA) using SuperScript IV Reverse Transcriptase (Invitrogen, Life Technologies) in accordance with the manufacturer's instructions. The cDNA was diluted to a working concentration of 5 ng μl^{-1} and stored at −20 °C until further use. qPCR was conducted using the TaqMan PCR system. Each reaction contained 5 ng of cDNA per replicate, and all reactions were performed in duplicate. For gene expression analysis, the expression levels of both housekeeping and target genes were quantified simultaneously. This was achieved by incorporating a VIC-conjugated probe specific for 18S rRNA and FAM-conjugated probes for the target genes of interest. Relative gene expression levels were calculated using the ΔΔCt method. The list of probes used is provided in the Supplementary Data Table 7.

Lactate quantification

Lactate concentrations were measured in the supernatant of SG organ cultures derived from multiple lobules from five patients with SjD with different degrees of histopathology focus scores, as well as in the submandibular SG tissue of both non-cannulated and cannulated mice, using the colourimetric L-Lactate Assay Kit (Abcam, ab65331).

For supernatant samples, after the completion of the organ culture, the supernatant was collected and stored at −80 °C until analysis. Lactate quantification was performed following the manufacturer's instructions. In brief, standards were prepared using known concentrations of L-lactate and incubated with the provided reaction mix. The absorbance of the samples and standards was measured at 450 nm using a microplate reader (Synergy HT). Lactate concentrations were determined by comparing the absorbance values to the standard curve generated from known concentrations.

For SG tissue samples, tissues from non-cannulated and cannulated mice were collected, weighed and immediately homogenized in standard buffer using a tissue homogenizer. The homogenized tissue was then centrifuged, and the resulting supernatant was used for lactate quantification. Lactate levels in the tissue supernatants were measured using the same procedure as described for the organ culture supernatants.

Immunofluorescence and immunohistochemical staining

Formalin-fixed, paraffin-embedded slides of SG biopsies from patients with SjD were selected based on the histological evidence of ELS[49]. Samples were classified as ELS+ (presence of ELS) or ELS− (absence of ELS). Tissue sections of 3 µm thickness were cut and mounted on polarized microscope slides. For hFFPE slides, deparaffinization was

Fig. 7 | Histological analysis, immune characterization and gene expression quantification in vehicle and 3C7 mAb-injected murine SGs. a Workflow of the mouse inducible ELS formation, following SGs cannulation. The experimental timeline shows that the AV was injected into the SG on day 0; on days 4 and 10, the 3C7 monoclonal anti-Slc5a12 antibody was administered. On day 14, SG tissues were collected for subsequent analyses. Post collection, tissues were processed for immunofluorescence and qPCR to assess relevant biomarkers and gene expression levels. **b**, Representative images of H&E staining of the whole SGs from vehicle-cannulated and 3C7 mAb-cannulated mice. Black arrows point to inflammatory foci (peri-ductal leukocytic infiltrates with more than 50 lymphocytes). **c**,**d**, Comparison between vehicle-cannulated and 3C7 mAb-cannulated mice ($n = 5$ or 6 per group) of focus score calculated on H&E images (**c**) and aggregate area fraction (% of SG area occupied by the inflammatory infiltrate), calculated on immunofluorescence images (**d**). **e**, Representative immunofluorescence staining of SG tissue sections from vehicle and 3C7 mAb-injected mice. CD3 (green) is used as a marker for T cells, B220 (red) is used as a marker for B cells and DAPI (blue) is used as a marker for nuclei. The images reveal the distribution and localization of T cells and B cells in the tissue and their segregation. Scale bars, 100 µm. **f**, Comparison between vehicle and 3C7 mAb-cannulated mice of the positive area for CD3 (T cells), B220 (B cells) and both (T cell–B cell intersection), respectively, as calculated from **e**. Data are presented as means; error bars, s.d. ($n = 4$ biological replicates per group). Statistical analysis was performed using an unpaired *t*-test. In **c**, **d** and **f**, box and whisker plots show the 75th and 25th percentiles of the data, and minimum and maximum values. Statistical significance was determined using a Mann–Whitney *U*-test (two-sided). **g**, Prevalence of segregated and non-segregated aggregates over the total number in vehicle and 3C7 mAb-cannulated mice, as calculated from **e**. **h**, qPCR analysis of gene expression levels for *Cxcr5, Cxcl13, Ccr7, Ccl19, Ltb, Ltbr, Il17, Il21* and *Il21r* in vehicle and 3C7 mAb-injected mice. Gene expression levels are normalized to a housekeeping gene and presented as relative expression levels. Data are expressed as means from $n = 8$–10 mice per group; error bars, s.d. Statistical significance was determined using a Mann–Whitney *U*-test and outliers were excluded by Grubb's test (*$P < 0.05$, **$P < 0.01$, ***$P < 0.001$, ****$P < 0.0001$).

https://doi.org/10.1038/s42255-025-01331-9

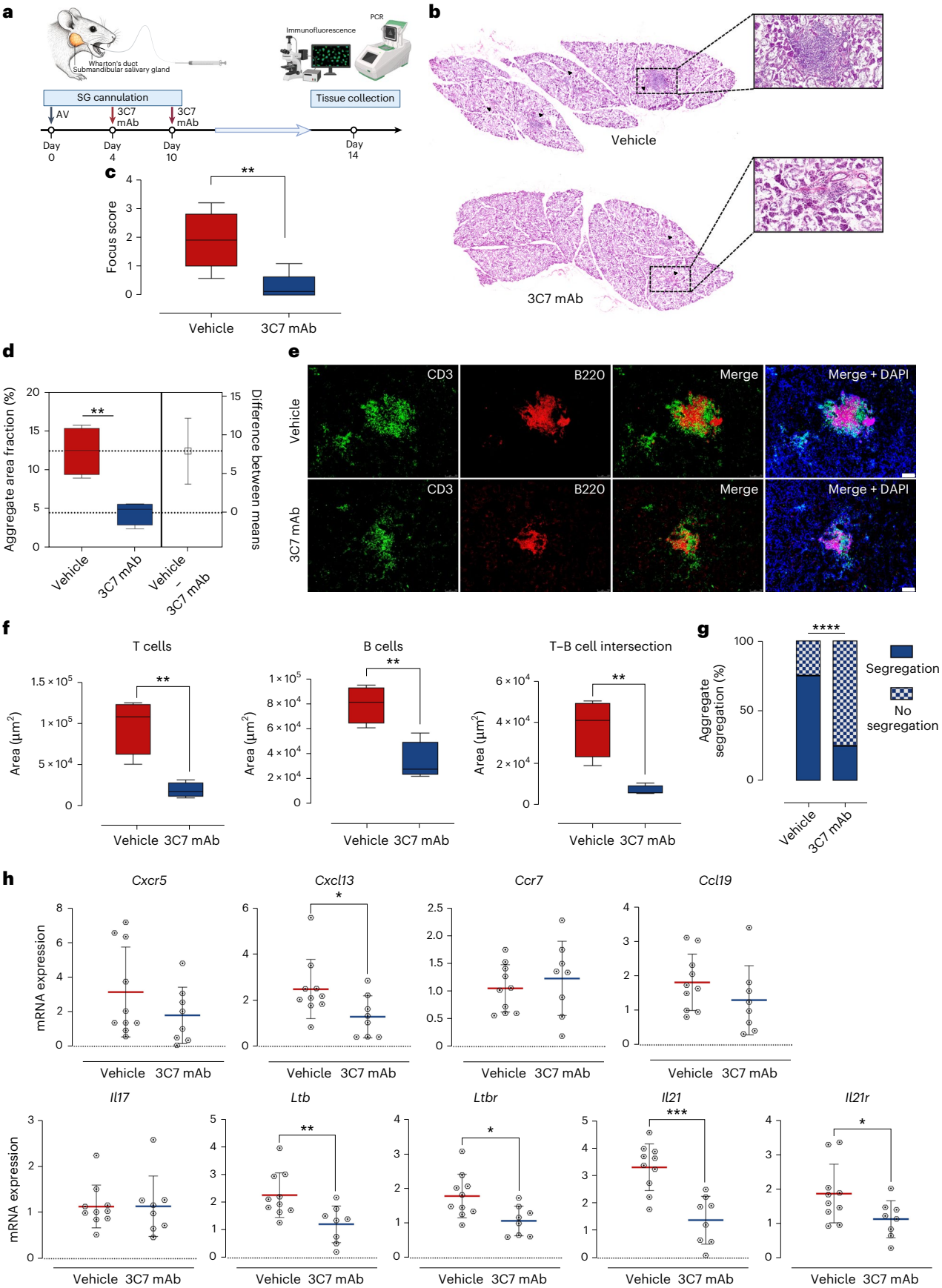

performed by immersion in xylene and rehydration through a series of graded ethanol solutions, followed by rinsing in distilled water. Heat-induced epitope retrieval was carried out using citrate buffer pH 6 (Agilent, S1699) at 95 °C for 30 min for staining combinations involving CD3 and SLC5A12, or using buffer pH 9 (Agilent, S2367) for staining combinations involving CD4 and SLC5A12. Following antigen retrieval, tissue sections were incubated in peroxidase blocking solution (Agilent) for 10 min to quench endogenous peroxidase activity, followed by protein blocking solution (Agilent) for 1 h at room temperature (22 ± 2 °C) to prevent non-specific binding. Primary antibodies were then added to the tissue sections and incubated for 1 h at room temperature. The details of the primary antibodies used are listed in Supplementary Data Table 8. After primary antibody incubation, slides were incubated with fluorochrome-conjugated secondary antibodies for 1 h at room temperature. Subsequently, slides were incubated with 5 µg ml^{-1} of 4′,6-diamidino-2-phenylindole (DAPI) in TBS (Life Technologies) for nuclear staining. Images were acquired using an Olympus IX81 fluorescence microscope with an Olympus digital camera (OrcaR-2). For the human images, whole-slide images were not acquired, and normalization to the total area was not applied. Instead, field images were specifically selected to include cell aggregates, either in the early stages of formation (initial stage-ELS) or fully organized (ELS+). Cell quantification was performed as the positive cell count per field.

For murine SG tissues, fresh-frozen murine SG tissues were used, with sections cut at 10 µm thickness using a cryostat. Hematoxilin and eosin (H&E) staining and direct double-immunofluorescence for CD3 and B220 were performed on sequential slides. The whole H&E slides were digitized using a Hamamatsu NanoZoomer S60 Slide Scanner at ×20 magnification. The digital analysis of the slides was conducted with the open-source software QuPath 0.6.0-rc3 (ref. 56).

For each H&E image, the digital imaging analysis included:

- Measurement of the total area of the gland, calculated using the software's area calculation tools by semi-manually determining the perimeter of the SG tissue.
- Count of the number of inflammatory foci (peri-ductal leukocytic infiltrates with more than 50 lymphocytes).

The focus score was calculated as follows: focus score = (infiltrate number / total SG area (mm^2)) × 4.

The image analysis of the immunofluorescence images was performed using cellSense software (Olympus). We identified regions on a pixel-by-pixel basis positive for DAPI and the markers of interest. To classify pixels as positive for DAPI and the markers of interest, we applied a global threshold on pixel intensities for the respective channels. The threshold values were assigned by a trained individual to ensure accurate identification of positively stained regions on all images. The global thresholds were implemented in QuPath[56], and the annotations were then exported as ImageJ regions of interest[57] and converted into simple features (sf library[58]) in the programming language R[59]. The area was quantified for regions in which markers of interest intersected the regions of positive pixels for the markers of interest. The areas were directly comparable between images, as the area of the images was fixed at 1,229,054.6934 $µm^2$. The areas were then compared, and a Wilcoxon statistical test was applied between the groups of interest. Aggregates segregation was evaluated by a trained individual, evaluating when CD3 and CD20 positive areas segregate in discrete areas.

The digital imaging analysis software was also used for the quantification of the aggregate area fraction on immunofluorescence images (CD3/B220) over the total area of the gland, measuring the fraction (%) of the total SG area occupied by the inflammatory aggregates. This complemented the information provided by the focus score, giving the dimension of the aggregates alongside the count provided by the focus score.

The area fraction of the aggregates was calculated as follows:

$$\text{Aggregate area fraction (\%)} = (\text{Aggregate area } (mm^2)/\text{Total SG area } (mm^2)) \times 100$$

For immunohistochemical staining of SLC5A12, human kidney tissue sections were first deparaffinized in xylene and rehydrated through a graded alcohol series. Antigen retrieval was performed by incubating the tissue sections in a citrate buffer (pH 6.0) and heating in a microwave for 10 min. After cooling, sections were washed in PBS and blocked with 5% normal goat serum for 1 h at room temperature to reduce non-specific binding. The primary antibody against SLC5A12 was applied to the tissue sections. The sections were incubated with the primary antibody overnight at 4 °C. After washing in PBS, sections were incubated with a secondary antibody conjugated to horseradish peroxidase for 1 h at room temperature. The staining signal was visualized using 3,3′-diaminobenzidine (DAB) as the chromogen, following the manufacturer's protocol. Counterstaining was performed using haematoxylin for 2 min to visualize tissue morphology. Sections were then dehydrated, cleared in xylene and mounted with a coverslip using mounting medium.

Acetylation array

CD4 T cells were isolated from mouse lymph nodes and spleen (Stemcell, 19852) and then activated and treated with lactate (10 mM) or left untreated over three time points: 12 h, 24 h and 48 h. Proteins were extracted with scioExtract buffer (Sciomics) using the extraction SOPs. After quality control of the samples, the bulk protein concentration was determined by bicinchoninic acid assay. The samples were labelled at an adjusted protein concentration for 2 h with scioDye 2. After 2 h, the reaction was stopped. Excess dye was removed and the buffer exchanged to PBS. All labelled protein samples were stored at −20 °C until use. The samples were analysed on scioDiscover antibody microarrays (Sciomics) targeting 1,352 different proteins with 1,821 antibodies. The arrays were blocked with scioBlock (Sciomics) on a Hybstation 4800 (Tecan). Subsequently, the samples were mixed with scioAcetyl detection mix, which enables detection of protein-specific acetylation, and incubated.

After incubation, the slides were thoroughly washed with 1× phosphate-buffered saline containing 0.05% Tween 20 (PBS-T), rinsed with 0.1 PBS-T and PBS, as well as with water, and subsequently dried with nitrogen. Slide scanning was conducted using a Powerscanner (Tecan) with constant instrument laser power and PMT settings. Spot segmentation was performed with GenePix Pro 6.0 (Molecular Devices). Acquired raw data were analysed using the linear models for microarray data (LIMMA) package of R-Bioconductor after uploading the median signal intensities. For normalization, a cyclic Loess normalization was applied. For analysis of the samples, a one-factorial linear model was fitted with LIMMA, resulting in a two-sided *t*-test or *F*-test based on moderated statistics. All presented *P* values were adjusted for multiple testing by controlling the false discovery rate according to Benjamini and Hochberg. Proteins were defined as differential for $|\log(\text{fold change})| > 0.5$ and an adjusted $P < 0.05$. Differences in protein abundance or acetylation level between different samples or sample groups are presented as $\log_2$(fold change).

Western blot analysis

CD4 T cells were isolated from the spleen and lymph nodes of the mice. Cells were activated and subsequently treated with 10 mM lactate or left untreated for 24 h. After treatment, cells were collected and lysed in RIPA buffer (50 mM Tris-HCl pH 7.4, 150 mM NaCl, 1% NP-40, 0.5% sodium deoxycholate, 0.1% SDS) supplemented with protease and phosphatase inhibitors. The supernatants were collected, and protein concentration was determined using the BCA Protein Assay Kit (Pierce). Equal amounts of protein (30 µg per sample) were mixed with Laemmli

sample buffer, boiled for 5 min, and separated by SDS–PAGE on a 10% polyacrylamide gel. The proteins were then transferred onto a PVDF membrane using a semi-dry transfer apparatus (Bio-Rad). Membranes were blocked with 5% non-fat dry milk in Tris-buffered saline with 0.1% Tween-20 (TBS-T) for 1 h at room temperature. The membranes were then incubated overnight at 4 °C with the following primary antibodies diluted in 5% BSA in TBS-T: Phospho-Stat3 (Tyr705) (Cell Signaling Technology, 1:1,000), Stat3 (Cell Signaling Technology, 1:1,000) and β-Actin (Cell Signaling Technology, 1:1,000). After washing three times with TBS-T, the membranes were incubated with horseradish peroxidase-conjugated secondary antibodies (anti-rabbit for Stat3 and pStat3, anti-mouse for β-Actin) (Cell Signaling Technology, 1:5,000) for 1 h at room temperature. The membranes were washed again three times with TBS-T, and the bound antibodies were detected using an enhanced chemiluminescence detection system (Thermo Scientific). The chemiluminescent signal was captured using a ChemiDoc Imaging System (Bio-Rad), and band intensities were quantified using ImageJ software (NIH). Data were analysed using GraphPad Prism software. Statistical significance was determined using a two-tailed Student's *t*-test, with $P < 0.05$ considered statistically significant. Results are presented as means ± s.e.m. of at least three independent experiments.

Cytokine measurements from ex vivo culture

PBMCs or SG (lip and parotid) biopsies, isolated from patients with SjD who had a positive lip biopsy for the histological evaluation for ELSs (confirmed by histology), were used for the in vitro culture. Each SG biopsy was cultured in RPMI 1640 medium supplemented with penicillin–streptomycin and 10% FBS for 24 h to allow for cell egression. Multiple samples from one MALT lymphoma parotidectomy and five SjD patient labial SG biopsies (2–8 lobules per patient) were tested. All culture supernatants were collected and frozen before cytokine analysis, as previously described. Cytokines were quantified using a customized multiplex liquid-phase immunoassay (Biolegend, LEGENDplex Human T_H Cytokine Panel), analysed with LEGENDplex data analysis software. A total of 12 human cytokines (IL-5, IL-13, IL-2, IL-6, IL-9, IL-10, IFNγ, TNF (TNFSF2), IL-17A, IL-17F, IL-4, IL-22) were simultaneously quantified. IL-21 levels were assessed with an ELISA kit (Biolegend, 433804) according to the manufacturer's instructions. Cytokine production by human $CD4^+$ and $CD8^+$ cells (Granzyme-B, IFNγ, IL-17A and IL-21) was assessed by flow cytometry on egressed cells from SG organ culture following the addition of GolgiStop in the final 4 h of culture.

Murine SGs were collected from non-cannulated mice (controls) and Adv-cannulated mice at 5 and 12 days post cannulation. The samples were analysed for T cell phenotype and IL-21 cytokine production. At 4 h before tissue collection, mice were injected in the tail vein with 100 µl of 2.5 mg ml^{-1} brefeldin A resuspended in PBS to enhance intracellular cytokine detection. Murine SGs were enzymatically digested in medium containing collagenase D (Roche) and DNase I (Sigma-Aldrich) for 15 min at 37 °C to obtain single-cell suspensions.

Cells from both human and murine samples were stained for surface antigens, fixed, permeabilized (using fixation-permeabilization buffer; eBioscience) and stained for intracellular cytokines as previously described. The details of the antibodies used for flow cytometry are listed in Supplementary Data Table 9. Data acquisition was performed on an LSR Fortessa II flow cytometer (BD Biosciences) and analysed using FlowJo (v.10) software. BD Cytometer Setup and Tracking Beads were routinely used to calibrate the cytometer. Single-stain controls and fluorescence minus one controls were included to enable compensation and precise gating, respectively. For human experiments, events were gated on viable cells, while murine samples were gated on viable $CD45^+$ cells. Where applicable, a dump channel was used to exclude non-relevant populations (V510/20 for human panels; R780/60 for murine panels).

The isolated PBMCs were cultured in RPMI 1640 medium supplemented with penicillin–streptomycin and 10% FBS. Cells were seeded in a 48-well plate at a density ranging from 200,000 to 300,000 cells per well. Cultures were maintained at 37 °C in a humidified atmosphere with 5% CO_2. For activation, PBMCs were treated with 0.2 µg ml^{-1} soluble anti-CD3 (clone UCHT-1) and anti-CD28 (clone CD28.2) monoclonal antibodies, and pre-incubated for 1 h with anti-SLC5A12 monoclonal or its isotype control before stimulation with lactate (10 mM) for 24 h. Cytokine production, specifically IL-21, was measured in the culture supernatant using an IL-21 ELISA kit (Biolegend, 433804) according to the manufacturer's instructions. IL-21 concentrations in the samples were determined by comparison to a standard curve generated using known concentrations of recombinant IL-21. Each sample was assayed in duplicate to ensure accuracy and reproducibility.

Statistical analysis

All statistical analyses were performed using GraphPad Prism 10. Data are presented as means ± s.d. unless otherwise indicated. Normality of data distributions was assessed using the Shapiro–Wilk test. The specific statistical tests used, sample size and post hoc corrections, where applicable, are provided in the corresponding figure legends.

Sample sizes were determined based on preliminary experiments and effect sizes observed in prior studies. Investigators were blinded to group allocation during data collection and analysis when feasible. All statistical tests were two-tailed, and $P < 0.05$ was considered statistically significant. No data were excluded unless predefined criteria were met.

Reporting summary

Further information on research design is available in the Nature Portfolio Reporting Summary linked to this article.

Data availability

The RNA-seq data are publicly accessible via the following repositories and web interfaces: i) observational disease-control cohort (SjD and sicca): https://doi.org/10.6084/m9.figshare.29211473, and https://sjogren.hpc.qmul.ac.uk/; ii) TRACTISS randomized clinical trial: ArrayExpress under accession code E-MTAB-15225, and https://tractiss.hpc.qmul.ac.uk/. The single-cell RNA-seq data are publicly accessible via the Gene Expression Omnibus under accession code GSE272409. Software code created for this study can be obtained at https://gitlab.bham.ac.uk/spillfsystems-mechanobiology-health-disease/els-analysis. All other data are available in the main text or in the Extended Data.

Code availability

Software code created for this study can be obtained at https://gitlab.bham.ac.uk/spillf-systems-mechanobiology-health-disease/els-analysis.

References

1. Bombardieri, M., Lewis, M. & Pitzalis, C. Ectopic lymphoid neogenesis in rheumatic autoimmune diseases. *Nat. Rev. Rheumatol.* **13**, 141–154 (2017).
2. Pitzalis, C., Jones, G. W., Bombardieri, M. & Jones, S. A. Ectopic lymphoid-like structures in infection, cancer and autoimmunity. *Nat. Rev. Immunol.* **14**, 447–462 (2014).
3. Petitprez, F. et al. B cells are associated with survival and immunotherapy response in sarcoma. *Nature* **577**, 556–560 (2020).
4. Cabrita, R. et al. Tertiary lymphoid structures improve immunotherapy and survival in melanoma. *Nature* **577**, 561–565 (2020).
5. Helmink, B. A. et al. B cells and tertiary lymphoid structures promote immunotherapy response. *Nature* **577**, 549–555 (2020).
6. Bombardieri, M. et al. Inducible tertiary lymphoid structures, autoimmunity, and exocrine dysfunction in a novel model of salivary gland inflammation in C57BL/6 mice. *J. Immunol.* **189**, 3767–3776 (2012).

7. Sène, D. et al. Ectopic germinal center-like structures in minor salivary gland biopsy tissue predict lymphoma occurrence in patients with primary Sjögren's syndrome. *Arthritis Rheumatol.* **70**, 1481–1488 (2018).
8. Theander, E. et al. Lymphoid organisation in labial salivary gland biopsies is a possible predictor for the development of malignant lymphoma in primary Sjögren's syndrome. *Ann. Rheum. Dis.* **70**, 1363–1368 (2011).
9. Thaunat, O. & Nicoletti, A. Comment on 'Activation-induced cytidine deaminase expression in follicular dendritic cell networks and interfollicular large B cells supports functionality of ectopic lymphoid neogenesis in autoimmune sialoadenitis and MALT lymphoma in Sjogren's syndrome'. *J. Immunol.* **180**, 2007–2008 (2008).
10. Voulgarelis, M. & Tzioufas, A. G. Pathogenetic mechanisms in the initiation and perpetuation of Sjögren's syndrome. *Nat. Rev. Rheumatol.* **6**, 529–537 (2010).
11. Drayton, D. L., Ying, X., Lee, J., Lesslauer, W. & Ruddle, N. H. Ectopic LTαβ directs lymphoid organ neogenesis with concomitant expression of peripheral node addressin and a HEV-restricted sulfotransferase. *J. Exp. Med.* **197**, 1153–1163 (2003).
12. Lucchesi, D. et al. Impaired interleukin-27-mediated control of $CD4^+$ T cell function impact on ectopic lymphoid structure formation in patients with Sjögren's syndrome. *Arthritis Rheumatol.* **72**, 1559–1570 (2020).
13. Jones, G. W. et al. Interleukin-27 inhibits ectopic lymphoid-like structure development in early inflammatory arthritis. *J. Exp. Med.* **212**, 1793–1802 (2015).
14. Barone, F. et al. IL-22 regulates lymphoid chemokine production and assembly of tertiary lymphoid organs. *Proc. Natl Acad. Sci. USA* **112**, 11024–11029 (2015).
15. Kohlgruber, A. C. et al. γδ T cells producing interleukin-17A regulate adipose regulatory T cell homeostasis and thermogenesis. *Nat. Immunol.* **19**, 464–474 (2018).
16. Peters, A. et al. Th17 cells induce ectopic lymphoid follicles in central nervous system tissue inflammation. *Immunity* **35**, 986–996 (2011).
17. Pikor, N. B. et al. Integration of Th17- and lymphotoxin-derived signals initiates meningeal-resident stromal cell remodeling to propagate neuroinflammation. *Immunity* **43**, 1160–1173 (2015).
18. Rangel-Moreno, J. et al. The development of inducible bronchus-associated lymphoid tissue depends on IL-17. *Nat. Immunol.* **12**, 639–646 (2011).
19. van Hooren, L. et al. Agonistic CD40 therapy induces tertiary lymphoid structures but impairs responses to checkpoint blockade in glioma. *Nat. Commun.* **12**, 4127 (2021).
20. Pontarini, E. et al. Unique expansion of IL-21^+ Tfh and Tph cells under control of ICOS identifies Sjögren's syndrome with ectopic germinal centres and MALT lymphoma. *Ann. Rheum. Dis.* **79**, 1588–1599 (2020).
21. Wieczorek, G. et al. Blockade of CD40–CD154 pathway interactions suppresses ectopic lymphoid structures and inhibits pathology in the NOD/ShiLtJ mouse model of Sjögren's syndrome. *Ann. Rheum. Dis.* **78**, 974–978 (2019).
22. Tsukamoto, H. et al. Aging-associated and CD4 T-cell-dependent ectopic CXCL13 activation predisposes to anti-PD-1 therapy-induced adverse events. *Proc. Natl Acad. Sci. USA* **119**, e2205378119 (2022).
23. Guo, J. et al. T follicular helper-like cells are involved in the pathogenesis of experimental autoimmune encephalomyelitis. *Front. Immunol.* **9**, 944 (2018).
24. O'Neill, L. A. J., Kishton, R. J. & Rathmell, J. A guide to immunometabolism for immunologists. *Nat. Rev. Immunol.* **16**, 553–565 (2016).
25. Buck, M. D., Sowell, R. T., Kaech, S. M. & Pearce, E. L. Metabolic instruction of immunity. *Cell* **169**, 570–586 (2017).
26. Tannahill, G. M. et al. Succinate is an inflammatory signal that induces IL-1β through HIF-1α. *Nature* **496**, 238–242 (2013).
27. Haas, R. et al. Lactate regulates metabolic and pro-inflammatory circuits in control of T cell migration and effector functions. *PLoS Biol.* **13**, e1002202 (2015).
28. Haas, R. et al. Intermediates of metabolism: from bystanders to signalling molecules. *Trends Biochem. Sci.* **41**, 460–471 (2016).
29. Llibre, A., Kucuk, S., Gope, A., Certo, M. & Mauro, C. Lactate: a key regulator of the immune response. *Immunity* **58**, 535–554 (2025).
30. Reina-Campos, M., Moscat, J. & Diaz-Meco, M. Metabolism shapes the tumor microenvironment. *Curr. Opin. Cell Biol.* **48**, 47–53 (2017).
31. Ho, P.-C. & Kaech, S. M. Reenergizing T cell anti-tumor immunity by harnessing immunometabolic checkpoints and machineries. *Curr. Opin. Immunol.* **46**, 38–44 (2017).
32. Colegio, O. R. et al. Functional polarization of tumour-associated macrophages by tumour-derived lactic acid. *Nature* **513**, 559–563 (2014).
33. Brand, A. et al. LDHA-associated lactic acid production blunts tumor immunosurveillance by T and NK cells. *Cell Metab.* **24**, 657–671 (2016).
34. Angelin, A. et al. Foxp3 reprograms T cell metabolism to function in low-glucose, high-lactate environments. *Cell Metab.* **25**, 1282–1293.e7 (2017).
35. Weyand, C. M., Zeisbrich, M. & Goronzy, J. J. Metabolic signatures of T cells and macrophages in rheumatoid arthritis. *Curr. Opin. Immunol.* **46**, 112–120 (2017).
36. Pucino, V., Bombardieri, M., Pitzalis, C. & Mauro, C. Lactate at the crossroads of metabolism, inflammation, and autoimmunity. *Eur. J. Immunol.* **47**, 14–21 (2017).
37. Certo, M., Tsai, C.-H., Pucino, V., Ho, P.-C. & Mauro, C. Lactate modulation of immune responses in inflammatory versus tumour microenvironments. *Nat. Rev. Immunol.* **21**, 151–161 (2021).
38. Certo, M., Marone, G., de Paulis, A., Mauro, C. & Pucino, V. Lactate: fueling the fire starter. *Wiley Interdiscip. Rev. Syst. Biol. Med.* **12**, e1474 (2020).
39. Certo, M., Llibre, A., Lee, W. & Mauro, C. Understanding lactate sensing and signalling. *Trends Endocrinol. Metab.* **33**, 722–735 (2022).
40. Amorini, A. M. et al. Serum lactate as a novel potential biomarker in multiple sclerosis. *Biochim. Biophys. Acta* **1842**, 1137–1143 (2014).
41. Srinivas, S. R. et al. Cloning and functional identification of slc5a12 as a sodium-coupled low-affinity transporter for monocarboxylates (SMCT2). *Biochem. J.* **392**, 655–664 (2005).
42. Halestrap, A. P. The monocarboxylate transporter family—structure and functional characterization. *IUBMB Life* **64**, 1–9 (2012).
43. Romero, M. et al. Immunometabolic effects of lactate on humoral immunity in healthy individuals of different ages. *Nat. Commun.* **15**, 7515 (2024).
44. Pucino, V. et al. Lactate buildup at the site of chronic inflammation promotes disease by inducing $CD4^+$ T cell metabolic rewiring. *Cell Metab.* **30**, 1055–1074.e8 (2019).
45. Subudhi, I. et al. Metabolic coordination between skin epithelium and type 17 immunity sustains chronic skin inflammation. *Immunity* **57**, 1665–1680.e7 (2024).
46. Shi, L. & Tu, B. P. Acetyl-CoA and the regulation of metabolism: mechanisms and consequences. *Curr. Opin. Cell Biol.* **33**, 125–131 (2015).
47. Shiboski, C. H. et al. 2016 American College of Rheumatology/European League Against Rheumatism classification criteria for primary Sjögren's syndrome: a consensus and data-driven methodology involving three international patient cohorts. *Arthritis Rheumatol.* **69**, 35–45 (2017).

48. Risselada, A. P. et al. The prognostic value of routinely performed minor salivary gland assessments in primary Sjögren's syndrome. *Ann. Rheum. Dis.* **73**, 1537–1540 (2014).
49. Pontarini, E. et al. Serum and tissue biomarkers associated with composite of relevant endpoints for Sjögren syndrome (CRESS) and Sjögren tool for assessing response (STAR) to B cell-targeted therapy in the trial of anti-B cell therapy in patients with primary Sjögren syndrome (TRACTISS). *Arthritis Rheumatol.* **76**, 763–776 (2024).
50. Lucchesi, D. et al. The use of digital image analysis in the histological assessment of Sjögren's syndrome salivary glands improves inter-rater agreement and facilitates multicentre data harmonisation. *Clin. Exp. Rheumatol.* **38**, 180–188 (2020).
51. Li, Z. et al. Lactate in the tumor microenvironment: a rising star for targeted tumor therapy. *Front Nutr.* **10**, 1113739 (2023).
52. Colafrancesco, S. et al. Inflammation in Sjögren disease induces salivary gland epithelial cells (SGECS) metabolic reprogramming: focus on glycolysis and its regulation of epithelial cell activation. *Ann. Rheum. Dis.* **83**, 862 (2024).
53. Sato, Y., Silina, K., van den Broek, M., Hirahara, K. & Yanagita, M. The roles of tertiary lymphoid structures in chronic diseases. *Nat. Rev. Nephrol.* **19**, 525–537 (2023).
54. Bombardieri, M. & Pitzalis, C. Ectopic lymphoid neogenesis and lymphoid chemokines in Sjogren's syndrome: at the interplay between chronic inflammation, autoimmunity and lymphomagenesis. *Curr. Pharm. Biotechnol.* **13**, 1989–1996 (2012).
55. Ganapathy, V. et al. Sodium-coupled monocarboxylate transporters in normal tissues and in cancer. *AAPS J.* **10**, 193–199 (2008).
56. Bankhead, P. et al. QuPath: open source software for digital pathology image analysis. *Sci. Rep.* **7**, 16878 (2017).
57. Schneider, C. A., Rasband, W. S. & Eliceiri, K. W. NIH Image to ImageJ: 25 years of image analysis. *Nat. Methods* **9**, 671–675 (2012).
58. Pebesma, E. Simple features for R: standardised support for spatial vector data. *R. J.* **10**, 439–446 (2018).
59. R Core Team. *R: A Language and Environment for Statistical Computing* (R Foundation for Statistical Computing, 2025); http://www.R-project.org/.

Acknowledgements

We acknowledge the contribution of the team at Janssen Pharmaceuticals (K. Silvils, D. Galbraith, H. Li, T. Lee, A. Halilovic, N. Rao and L.-Y. Hao) in the generation of the RNA-seq data (Fig. 1f and Extended Data Fig. 1c) that were used for the development of the R Shiny App. We also extend our thanks to C. Frezza, N. Jones and their respective teams for their invaluable feedback and critical review that greatly enhanced this paper. We are also grateful to the BMSU staff at the University of Birmingham for their support with animal experiments, which were crucial for this study. Figs. 1a, 3a, 4a, 5a, 6a and 7a created with Biorender.com. This study was principally funded by the Medical Research Council Project Grant MR/T016736/1 to C.M. and M.B. During the tenure of this Project Grant, further funding to C.M. has supported the study: a University of Brimingham Professorial Fellowship for relocation from Queen Mary University of London to the University of Birmingham; the British Heart Foundation Senior Basic Science Research Fellowship FS/SBSRF/22/31031; and the UNION-HORIZON-MSCA-DN-2024-111167421. This work was supported by project grants from the British Sjögren's Syndrome Association (research grant to E.P.), Barts Charity Seed Grant for Research (grant G-002367 to M.B.), the Versus Arthritis Foundation (fellowship grant 21753 to E.P.) and the National Institute for Health and Care Research (NIHR) Musculoskeletal Biomedical Research Centre (to M.B.). This work was also supported by the National Institute for Health Research Barts Biomedical Research Centre (NIHR203330 to M.B.). This project has also received funding from the Innovative Medicines Initiative 2 Joint Undertaking (JU) NECESSITY (under grant agreement no. 806975). The JU receives support from the European Union's Horizon 2020 Research and Innovation Programme and EFPIA. The present article reflects only the author's view, and the JU is not responsible for any use that may be made of the information it contains. F.S. is funded by a UKRI Future Leaders Fellowship (MR/T043571/1). S.G.G. was supported in part by the EPSRC Centre for Doctoral Training in Topological Design, funded by the UK Engineering and Physical Sciences Research Council (grant EP/S02297X/1) and in part by the University of Birmingham. B.A.F. has received support from the NIHR Birmingham Biomedical Research Centre (NIHR 203326). The views expressed in this publication are those of the authors and not necessarily those of the NHS, the NIHR or the Department of Health.

Author contributions

M.C., E.P., M.B. and C.M. conceptualized the study. M.C., E.P., D.L., D.A., S.N. and C.G.S. developed the methodology. M.C., E.P. and R.S. performed the investigation. M.C., E.P., S.G.G., J.D.T., G.C., S.C., J.C. and R.S. conducted the formal analysis. C.S., B.A.F., F.S., M.B. and C.M. supervised the research. M.C., E.P., M.B. and C.M. wrote the original draft of the paper; all authors contributed to paper review, editing and approved the final version to be published.

Competing interests

C.M. is a founder and CSO of Solute Guard Therapeutics (SGTx). M.B. is a member of the scientific advisory board of SGTx. The other authors declare no competing interests.

Additional information

Extended data is available for this paper at https://doi.org/10.1038/s42255-025-01331-9.

Supplementary information The online version contains supplementary material available at https://doi.org/10.1038/s42255-025-01331-9.

Correspondence and requests for materials should be addressed to Michelangelo Certo, Michele Bombardieri or Claudio Mauro.

Peer review information *Nature Metabolism* thanks Navdeep Chandeland and the other, anonymous, reviewer(s) for their contribution to the peer review of this work. Primary Handling Editor: Alfredo Giménez-Cassina, in collaboration with the *Nature Metabolism* team.

[1]Department of Inflammation and Ageing, School of Infection, Inflammation and Immunology, College of Medicine and Health, University of Birmingham, Birmingham, UK. [2]Experimental Medicine and Rheumatology, William Harvey Research Institute, Queen Mary University of London, London, UK. [3]School of Mathematics, University of Birmingham, Birmingham, UK. [4]Sciomics GmbH, Neckargemünd, Germany. [5]Department of Translational Medicine, University of Piemonte Orientale (UPO), Novara, Italy. [6]Department of Physics and Astronomy, University of Catania, Catania, Italy. [7]Department of Biomedical Sciences, Humanitas University, Pieve Emanuele, and Rheumatology and Clinical Immunology, Istituto di Ricovero e Cura a Carattere Scientifico, IRCCS Humanitas Research Hospital, Rozzano, Italy. [8]NIHR Birmingham Biomedical Research Centre, University Hospitals Birmingham NHS Foundation Trust and University of Birmingham, Birmingham, UK. [9]Present address: Birmingham Tissue Analytics, Institute of Translational Medicine, University of Birmingham, Birmingham, UK. [10]Present address: Propath UK Limited, Hereford, UK. [11]These authors contributed equally: Michelangelo Certo, Elena Pontarini. [12]These authors jointly supervised this work: Michele Bombardieri, Claudio Mauro. ✉e-mail: m.certo@bham.ac.uk; m.bombardieri@qmul.ac.uk; c.mauro@bham.ac.uk

https://doi.org/10.1038/s42255-025-01331-9

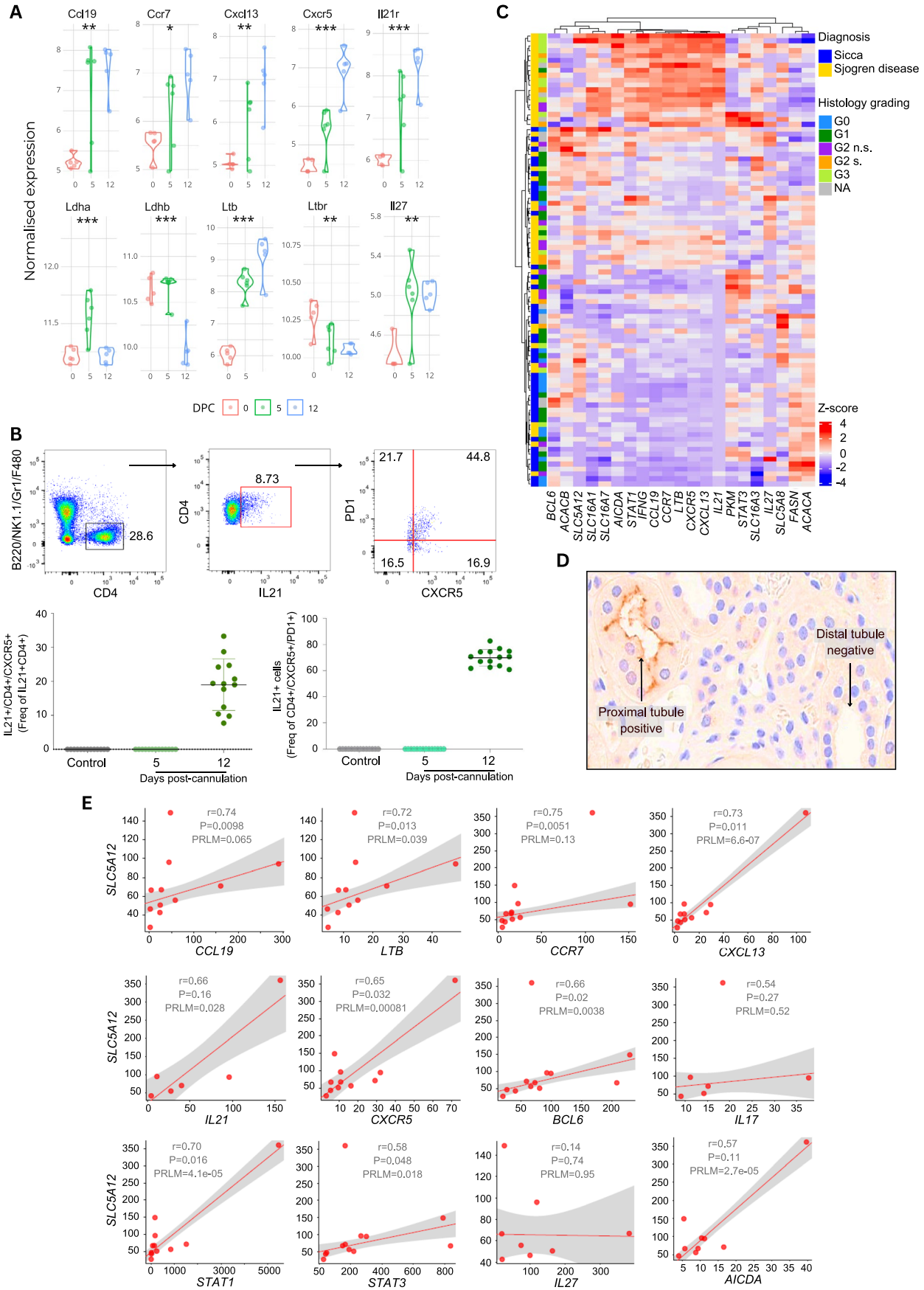

Extended Data Fig. 1 | See next page for caption.

https://doi.org/10.1038/s42255-025-01331-9

Extended Data Fig. 1 | Gene expression and correlation analysis of inflammatory mediators in salivary glands. (a) Expression levels of selected genes related to inflammatory mediators involved in ectopic lymphoid structure (ELS) formation and function in murine salivary glands collected at 0-, 5-, and 12-days post-cannulation. Adjusted p-values calculated by DESeq2 (*$p < 0.05$, **$p < 0.01$, ***$p < 0.001$, ****$p < 0.0001$). **(b)** Flow cytometry gating strategy showing the phenotype of $CD4^+$ T cells producing IL21 (top panel). Frequency of IL21-producing T CD4+ cells with a Tfh-phenotype (CD4 + / CXCR5 + , bottom left panel), and frequency of IL21+ cells in the Tfh cell population (CD4 + / CXCR5 + /PD1 + , bottom right panel) in murine salivary glands collected at 0-, 5-, and 12-days post-cannulation.Data are expressed as mean ± SD from n = 13 glands per group. **(c)** Unsupervised heatmap of differentially expressed genes (DEGs) comparing SjD patients versus sicca controls. **(d)** Immunohistochemistry staining of human kidney tissue using anti-SLC5A12 antibody. **(e)** Correlation plots of SLC5A12 expression with inflammatory mediator genes relevant to ELS formation and function. Gene expression was evaluated using real-time PCR (n = 18). Spearman correlation coefficient (r) and p-values (two-sided) are shown.

https://doi.org/10.1038/s42255-025-01331-9

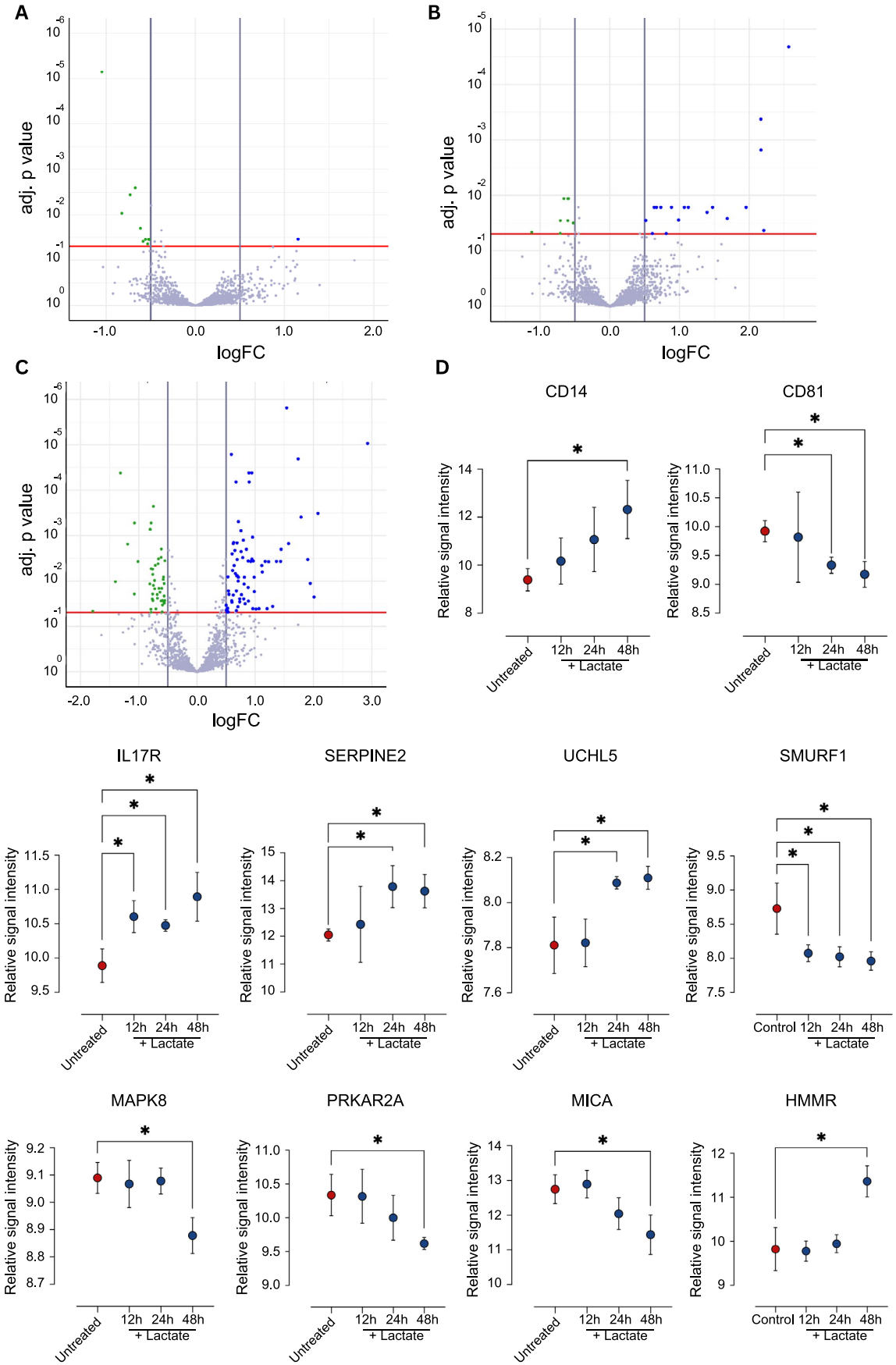

Extended Data Fig. 2 | See next page for caption.

https://doi.org/10.1038/s42255-025-01331-9

Extended Data Fig. 2 | Protein expression analysis. Volcano plots illustrating the results of the differential expression analysis comparing untreated and lactate-treated (12 h **a**, 24 h **b**, and 48 h **c**) CD4 T cells. Each point on the plot represents a single protein. P values (adjusted for multiple testing) and corresponding log-fold changes (logFC) are shown. A significance level of adj. p-value = 0.05 is indicated as a horizontal red line. The logFC cutoffs are indicated as vertical lines. Proteins with a positive logFC had a higher abundance in lactate-treated samples, proteins with a negative value in untreated samples. Proteins indicated with green points feature a logFC > 1, while not reaching the significance threshold. **(d)** Individual array values for a set of differential proteins in untreated and lactate-treated (12 h, 24 h, and 48 h) CD4 T cells. Each sample is measured by four replicate spots per array. For analysis of the samples a one-factorial linear model was fitted with LIMMA resulting in a two-sided t-test. Data are presented as mean values +/- SD (*$p < 0.05$, n = 3 biological replicates).

https://doi.org/10.1038/s42255-025-01331-9

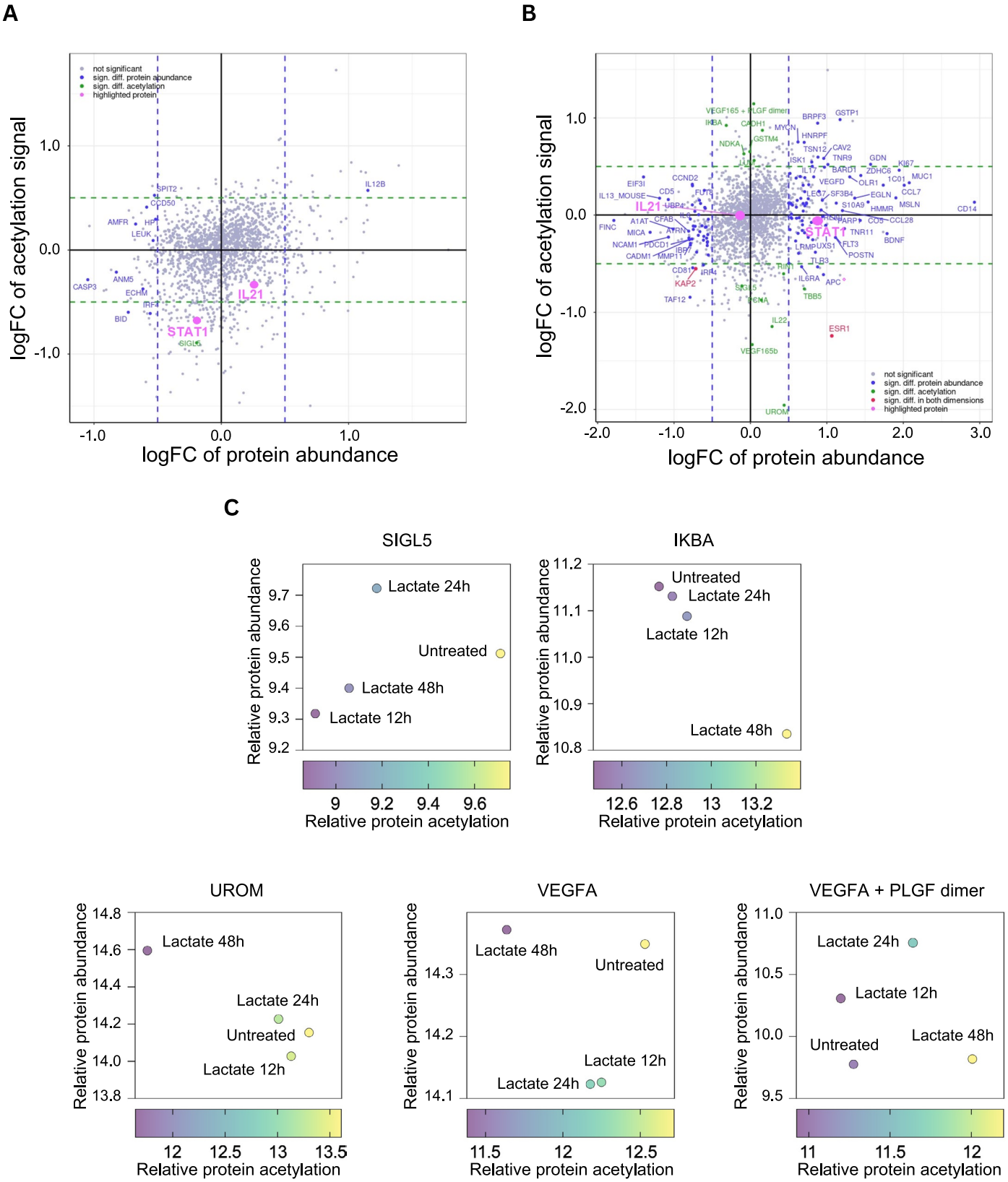

Extended Data Fig. 3 | Differential protein abundance versus acetylation level. Overview of differences in protein abundance as well as acetylation levels between untreated and lactate-treated (12 h **a**, and 48 h **b**) CD4 T cells. Proteins with a positive logFC (protein, x-axis) were more abundant in lactate-treated samples, while proteins with a negative logFC were more abundant in untreated samples. For proteins with a positive logFC (acetyl, y-axis), higher acetylation signals were obtained in lactate-treated samples. For proteins with a negative logFC, higher acetylation signals were obtained in untreated samples. **(c)** Individual array values for a set of differential proteins in untreated and lactate-treated (48 h) CD4 T cells.

https://doi.org/10.1038/s42255-025-01331-9

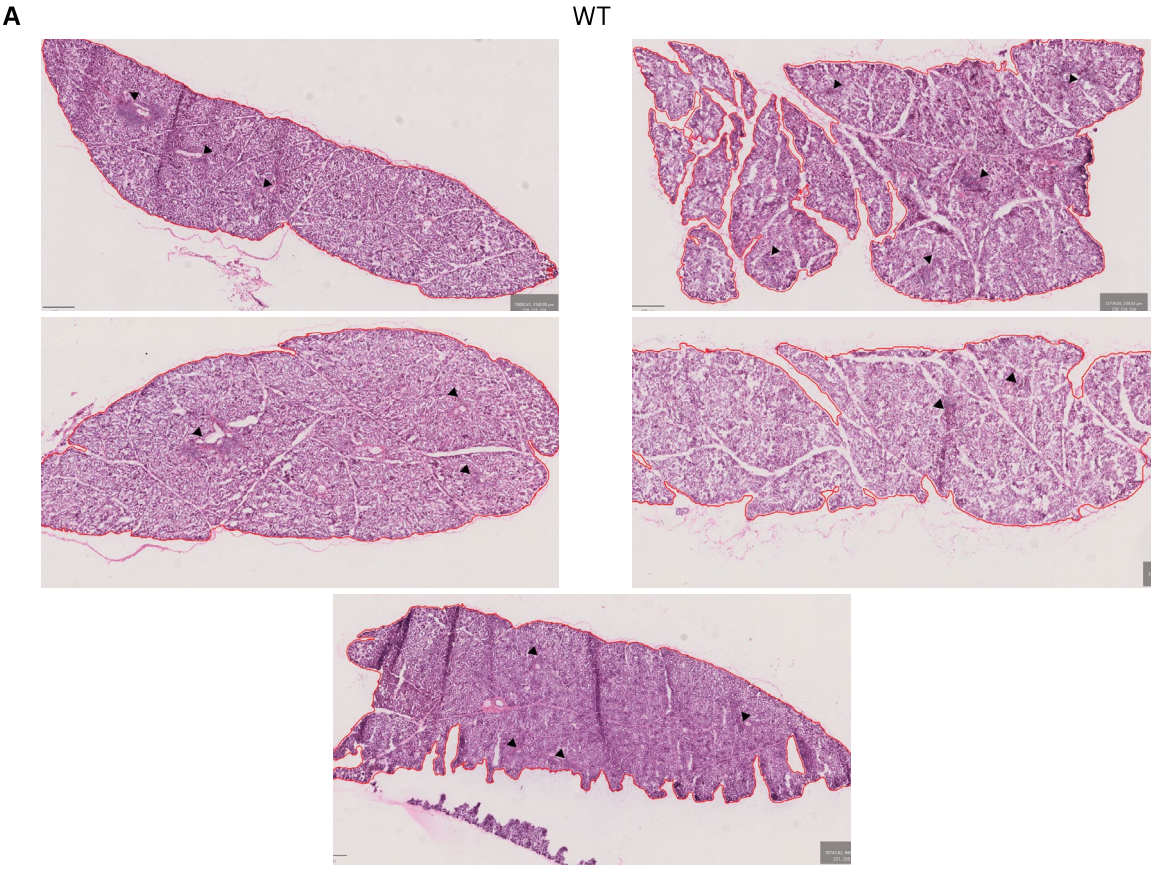

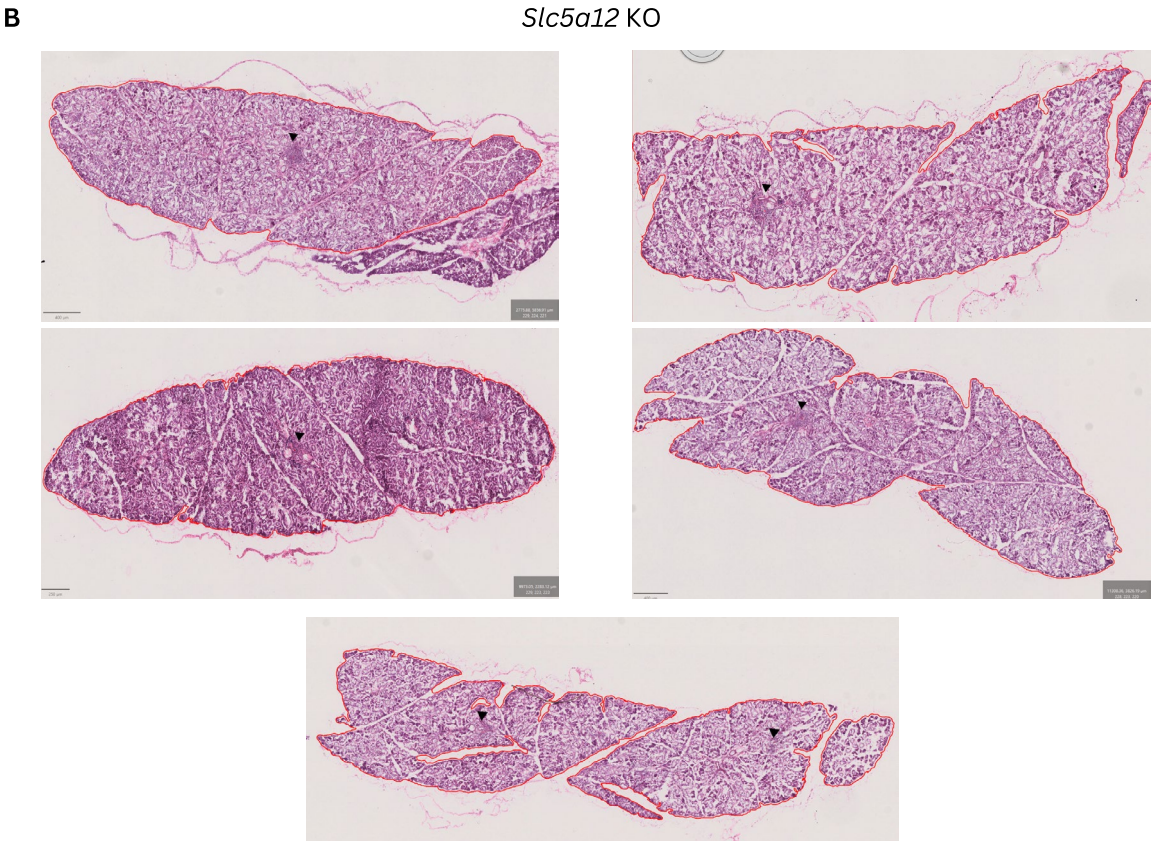

Extended Data Fig. 4 | Comparison of inflammatory foci in salivary glands of WT and *Slc5a12* KO mice. Whole-slide images of hematoxylin and eosin (H&E) staining of salivary glands from WT **(a)** and Slc5a12 KO **(b)** mice (n = 5 per group), showing differences in the inflammatory foci (peri-ductal leukocytic infiltrates containing more than 50 lymphocytes, black arrows).

https://doi.org/10.1038/s42255-025-01331-9

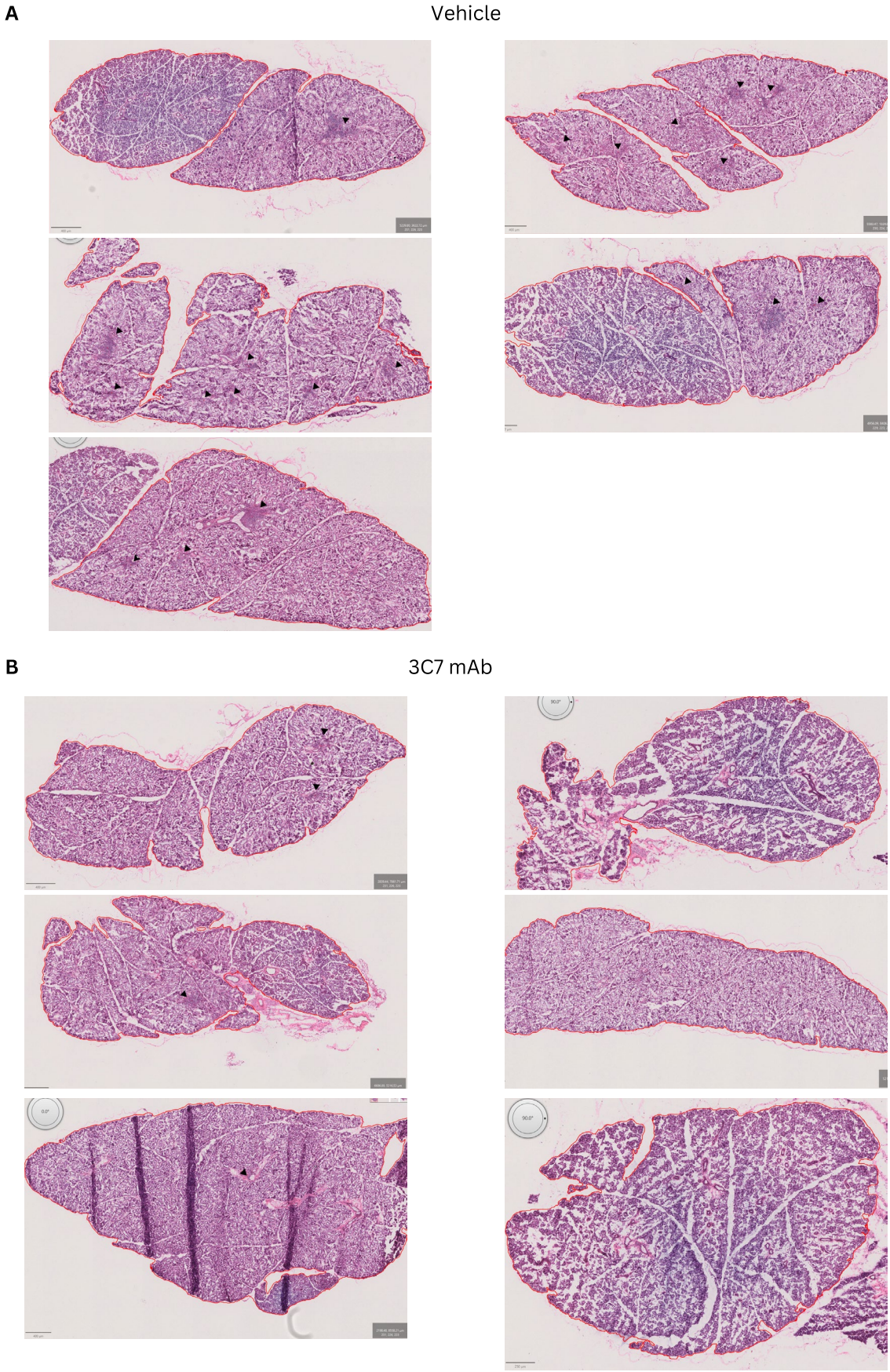

Extended Data Fig. 5 | Comparison of inflammatory foci in salivary glands of vehicle-cannulated and 3C7 mAb-cannulated mice. Whole-slide images of hematoxylin and eosin (H&E) staining of salivary glands from vehicle-cannulated **(a)** and 3C7 mAb-cannulated **(b)** mice (n = 5/6 pr group), showing differences in inflammatory foci (peri-ductal leukocytic infiltrates containing more than 50 lymphocytes, black arrows).

https://doi.org/10.1038/s42255-025-01331-9

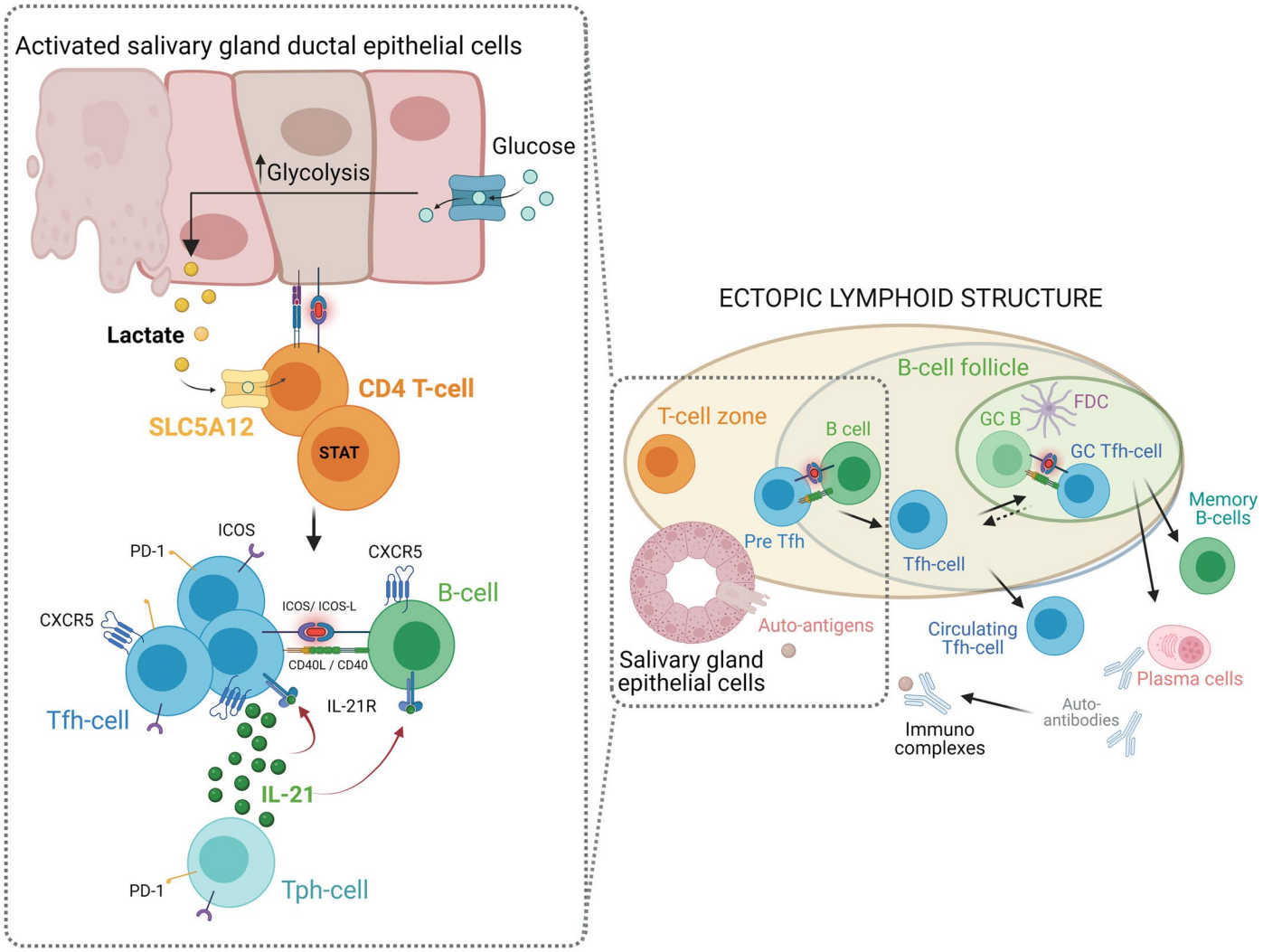

Extended Data Fig. 6 | Mechanisms of ectopic lymphoid structure formation in salivary glands. The figure illustrates the proposed impact of lactate accumulation on T cell activation and the development of ectopic lymphoid structures in SjD SGs. (Left panel) Activated stromal cells, such as ductal epithelial cells, and infiltrating immune cells increase glycolysis, leading to lactate production and release into the microenvironment. $CD4^+$ T cells uptake lactate via the SLC5A12 transporter. Lactate stimulates IL21 production by Tfh and Tph cells, driving B-cell activation and differentiation. (Right panel) Within the ectopic lymphoid structure, B cells organize into follicles supported by follicular dendritic cells (FDCs). Tfh cells provide help to B cells, leading to the production of autoantibodies and the generation of plasma cells and memory B cells. Autoantigens from the salivary gland epithelial cells contribute to the formation of immune complexes, perpetuating the autoimmune response.

nature portfolio

Corresponding author(s): Michelangelo Certo, Michele Bombardieri, Claudio Mauro

Last updated by author(s): May 5, 2025

Reporting Summary

Nature Portfolio wishes to improve the reproducibility of the work that we publish. This form provides structure for consistency and transparency in reporting. For further information on Nature Portfolio policies, see our Editorial Policies and the Editorial Policy Checklist.

Statistics

For all statistical analyses, confirm that the following items are present in the figure legend, table legend, main text, or Methods section.

n/a	Confirmed	
☐	☒	The exact sample size (*n*) for each experimental group/condition, given as a discrete number and unit of measurement
☒	☐	A statement on whether measurements were taken from distinct samples or whether the same sample was measured repeatedly
☐	☒	The statistical test(s) used AND whether they are one- or two-sided *Only common tests should be described solely by name; describe more complex techniques in the Methods section.*
☒	☐	A description of all covariates tested
☐	☒	A description of any assumptions or corrections, such as tests of normality and adjustment for multiple comparisons
☐	☒	A full description of the statistical parameters including central tendency (e.g. means) or other basic estimates (e.g. regression coefficient) AND variation (e.g. standard deviation) or associated estimates of uncertainty (e.g. confidence intervals)
☐	☒	For null hypothesis testing, the test statistic (e.g. *F*, *t*, *r*) with confidence intervals, effect sizes, degrees of freedom and *P* value noted *Give P values as exact values whenever suitable.*
☒	☐	For Bayesian analysis, information on the choice of priors and Markov chain Monte Carlo settings
☒	☐	For hierarchical and complex designs, identification of the appropriate level for tests and full reporting of outcomes
☒	☐	Estimates of effect sizes (e.g. Cohen's *d*, Pearson's *r*), indicating how they were calculated

Our web collection on statistics for biologists contains articles on many of the points above.

Software and code

Policy information about availability of computer code

Data collection	Data collection was conducted without the use of software.
Data analysis	- CellSense software (Olympus) - QuPath 0.6.0-rc3 - Graphpad Prism 10 - R (v.4.2.1) within RStudio environment (v1.2.5042) - FlowJo V.10 - LEGENDplex™ Data Analysis Software

For manuscripts utilizing custom algorithms or software that are central to the research but not yet described in published literature, software must be made available to editors and reviewers. We strongly encourage code deposition in a community repository (e.g. GitHub). See the Nature Portfolio guidelines for submitting code & software for further information.

Data

Policy information about availability of data

All manuscripts must include a data availability statement. This statement should provide the following information, where applicable:

- Accession codes, unique identifiers, or web links for publicly available datasets
- A description of any restrictions on data availability
- For clinical datasets or third party data, please ensure that the statement adheres to our policy

The RNA-seq data are publicly accessible through the following web interfaces:
i) Observational disease-control cohort (Sjogren's disease and sicca): https://sjogren.hpc.qmul.ac.uk/
ii) TRACTISS randomized clinical trial: https://tractiss.hpc.qmul.ac.uk/
iii) Software code created for this study can be obtained at: https://gitlab.bham.ac.uk/spillfsystems-mechanobiology-health-disease/els-analysis
All other data are available in the main text or in the Extended Data.

Research involving human participants, their data, or biological material

Policy information about studies with human participants or human data. See also policy information about sex, gender (identity/presentation), and sexual orientation and race, ethnicity and racism.

Reporting on sex and gender	Information on sex and/or gender of the human participants has not been reported in the current manuscript. Sex of the QMUL cohort participants according to hospital notes is reported below (see population characteristics) and was previously reported for the TRACTISS trial in the original manuscripts (see population characteristics below)
Reporting on race, ethnicity, or other socially relevant groupings	Information on race and/or ethnicity of the human participants has not been reported in the current manuscript
Population characteristics	QMUL cohort characteristic are reported below Sjogren (n=51) Sicca (n=42) Sex F/M 43 /8 37 /5 TRACTISS trial general population characteristics are extensively reported in Age in years Mean [Median] (SD) 54.84 [55.00] 13.31 56.62 [56.50] 13.02 Disease duration in years Mean [Median] (SD) 7.20 [6.00] 6.19 4.65 [2.00] 5.34 ESSDAI at biopsy Mean [Median] (SD) 5.89 [5.00] 4.94 / Anti-Ro (Ro/SSA) Positive of total (%) 32 /51 (62.75%) 0 /38 (0%) Anti-La (La/SSB) Positive of total (%) 21 /51 (41.18%) 0 /38 (0%) Rheumatoid factor (RF) Positive of total (%) 25 /47 (57.44%) 2 /37 (5.41%) Anti-Nuclear antibody (ANA) Positive of total (%) 29 /37 (78.38%) 12 /41 (29.27%) Serum IgG (g/L) Mean [Median] (SD) 15.75 [13.85] 7.27 11.01 [11.20] 2.57 Serum IgA (g/L) Mean [Median] (SD) 2.96 [2.51] 1.64 2.75 [2.30] 2.83 Serum IgM (g/L) Mean [Median] (SD) 1.43 [1.18] 1.03 1.30 [1.06] 0.80 Serum C3 (g/L) Mean [Median] (SD) 1.23 [1.20] 0.29 1.29 [1.32] 0.21 Serum C4 (g/L) Mean [Median] (SD) 0.25 [0.25] 0.11 0.29 [0.27] 0.09 ELS Negative / Positive/ NA 23 / 24 / 4 / TRACTISS total cohort characteristics are extensively reported in "Randomized Controlled Trial of Rituximab and Cost-Effectiveness Analysis in Treating Fatigue and Oral Dryness in Primary Sjogren's Syndrome. Bowman SJ, Everett CC, O'Dwyer JL, Emery P, Pitzalis C, Ng WF, Pease CT, Price EJ, Sutcliffe N, Gendi NST, Hall FC, Ruddock SP, Fernandez C, Reynolds C, Hulme CT, Davies KA, Edwards CJ, Lanyon PC, Moots RJ, Roussou E, Giles IP, Sharples LD, Bombardieri M. Arthritis Rheumatol. 2017 Jul;69(7):1440-1450. doi: 10.1002/art.40093. Epub 2017 Jun 5" TRACTISS salivary gland biopsy cohort characteristics are extensively reported in "Serum and Tissue Biomarkers Associated With Composite of Relevant Endpoints for Sjögren Syndrome (CRESS) and Sjögren Tool for Assessing Response (STAR) to B Cell-Targeted Therapy in the Trial of Anti-B Cell Therapy in Patients With Primary Sjögren Syndrome (TRACTISS). Pontarini E, Sciacca E, Chowdhury F, Grigoriadou S, Rivellese F, Murray-Brown WJ, Lucchesi D, Fossati-Jimack L, Nerviani A, Jaworska E, Ghirardi GM, Giacomassi C, Emery P, Ng WF, Sutcliffe N, Everett C, Fernandez C, Tappuni A, Seror R, Mariette X, Porcher R, Cavallaro G, Pulvirenti A, Verstappen GM, de Wolff L, Arends S, Bootsma H, Lewis MJ, Pitzalis C, Bowman SJ, Bombardieri M; Trial for Anti–B Cell Therapy in Patients With Primary Sjögren Syndrome Study Research Group.

Arthritis Rheumatol. 2024 May;76(5):763-776. doi: 10.1002/art.42772. Epub 2024 Feb 15"

Recruitment

The cross-sectional QMUL cohort consists of a monocentric cohort of consecutive patients with a diagnosis of Sjogren's disease or sicca/non specific chronic sialoadenitis who consented to donate labial salivary gland tissue for research obtained during diagnostic labial salivary gland biopsies.
The TRACTISS cohort consists of a multicentric UK cohort of patients with Sjogren's disease enrolled in the randomised double-blind placebo controlled TRACTISS trial. The TRACTISS trial design, with inclusion and exclusion criteria have been extensively presented in the original manuscript reporting the results of the trial in "Randomized Controlled Trial of Rituximab and Cost-Effectiveness Analysis in Treating Fatigue and Oral Dryness in Primary Sjogren's Syndrome.
Bowman SJ, Everett CC, O'Dwyer JL, Emery P, Pitzalis C, Ng WF, Pease CT, Price EJ, Sutcliffe N, Gendi NST, Hall FC, Ruddock SP, Fernandez C, Reynolds C, Hulme CT, Davies KA, Edwards CJ, Lanyon PC, Moots RJ, Roussou E, Giles IP, Sharples LD, Bombardieri M. Arthritis Rheumatol. 2017 Jul;69(7):1440-1450. doi: 10.1002/art.40093. Epub 2017 Jun 5"

Ethics oversight

The human study including disease-control cohort (sicca/Sjogren's disease) was approved by the Research Ethics Committee, reference 17/WS/0172 and 05/Q0702/1. The TRACTISS randomized clinical trial including the collection of biological samples was approved by Leeds Research Ethics Committee 10/H1307/99.

Note that full information on the approval of the study protocol must also be provided in the manuscript.

Field-specific reporting

Please select the one below that is the best fit for your research. If you are not sure, read the appropriate sections before making your selection.

☒ Life sciences ☐ Behavioural & social sciences ☐ Ecological, evolutionary & environmental sciences

For a reference copy of the document with all sections, see nature.com/documents/nr-reporting-summary-flat.pdf

Life sciences study design

All studies must disclose on these points even when the disclosure is negative.

Sample size

The QMUL cohort is a consecutive cross-sectional observational cohort of 51 Sjogren and 42 sicca patients undergoing diagnostic salivary gland biopsies who consented to donate additional tissue for research and for which sufficient material was obtained for bulk RNA sequencing. No formal power calculations were performed.
The TRACTISS trial sample size underwent formal power calculations as originally reported in "The TRACTISS protocol: a randomised double blind placebo controlled clinical trial of anti-B-cell therapy in patients with primary Sjögren's Syndrome. Brown S, Navarro Coy N, Pitzalis C, Emery P, Pavitt S, Gray J, Hulme C, Hall F, Busch R, Smith P, Dawson L, Bombardieri M, Wan-Fai N, Pease C, Price E, Sutcliffe N, Woods C, Ruddock S, Everett C, Reynolds C, Skinner E, Poveda-Gallego A, Rout J, Macleod I, Rauz S, Bowman S; TRACTISS trial team.
BMC Musculoskelet Disord. 2014 Jan 17;15:21. doi: 10.1186/1471-2474-15-21"

Data exclusions

Salivary gland biopsies for which either i) not sufficient RNA was available and/or ii) RNA quality as assessed by RIN or iii) did not pass quality control prior or after RNA sequencing were excluded from the study. The data presented from the cohort of 51 Sjogren and 42 sicca patients comprise patients who passed all the above quality control steps.

Replication

No bulk RNA sequencing data replication was available for this study.

Randomization

The TRACTISS trial involved randomization to either Rituximab or placebo as described in "The TRACTISS protocol: a randomised double blind placebo controlled clinical trial of anti-B-cell therapy in patients with primary Sjögren's Syndrome. Brown S, Navarro Coy N, Pitzalis C, Emery P, Pavitt S, Gray J, Hulme C, Hall F, Busch R, Smith P, Dawson L, Bombardieri M, Wan-Fai N, Pease C, Price E, Sutcliffe N, Woods C, Ruddock S, Everett C, Reynolds C, Skinner E, Poveda-Gallego A, Rout J, Macleod I, Rauz S, Bowman S; TRACTISS trial team.
BMC Musculoskelet Disord. 2014 Jan 17;15:21. doi: 10.1186/1471-2474-15-21"

Blinding

The TRACTISS trial is a double blinded trial as described in "The TRACTISS protocol: a randomised double blind placebo controlled clinical trial of anti-B-cell therapy in patients with primary Sjögren's Syndrome. Brown S, Navarro Coy N, Pitzalis C, Emery P, Pavitt S, Gray J, Hulme C, Hall F, Busch R, Smith P, Dawson L, Bombardieri M, Wan-Fai N, Pease C, Price E, Sutcliffe N, Woods C, Ruddock S, Everett C, Reynolds C, Skinner E, Poveda-Gallego A, Rout J, Macleod I, Rauz S, Bowman S; TRACTISS trial team. BMC Musculoskelet Disord. 2014 Jan 17;15:21. doi: 10.1186/1471-2474-15-21"

Reporting for specific materials, systems and methods

We require information from authors about some types of materials, experimental systems and methods used in many studies. Here, indicate whether each material, system or method listed is relevant to your study. If you are not sure if a list item applies to your research, read the appropriate section before selecting a response.

Materials & experimental systems

n/a	Involved in the study
☐	☒ Antibodies
☒	☐ Eukaryotic cell lines
☒	☐ Palaeontology and archaeology
☐	☒ Animals and other organisms
☐	☒ Clinical data
☒	☐ Dual use research of concern
☒	☐ Plants

Methods

n/a	Involved in the study
☒	☐ ChIP-seq
☐	☒ Flow cytometry
☒	☐ MRI-based neuroimaging

Antibodies

Antibodies used

Antibodies for histology

Primary Antibody	Conjugation	Source	Catalogue	Clone	Dilution
CD3 (human)	None	Agilent-Dako	M7254	F7.2.38	1:100
CD3 (mouse)	Alexa Fuor 488	Biolegend	100210	17A2	1:100
CD4 (human)	None	Agilent-Dako	M7310	4B12	1:100
CD20 (human)	None	Agilent-Dako	M0755	L26	1:400
B220 (mouse)	Alexa Fuor 647	Biolegend	103226	RA3-6B2	1:200
SLC5A12 (human)	None	Sigma-Aldrich	HPA045181	polyclonal	1:50

Antibodies for flowcytometry

Antibodies for flowcytometry staining for human samples

Antigen	Fluorochrome	Filter	Clone	Company	Cat. Numb	Batch	Working dilution (ul)
Surface:							
Zombie Viable Dye	Aqua	V525/50					
CD14	BV510	V525/50	M5E2	BioLegend	301842	B261483	2.5
CD19	BV510	V525/50	HIB19	BioLegend	302242	B221987	1
CD56	BV510	V525/50	HCD56	Biolegend	318340	B235441	2
CXCR5	BV605	V610/20	J252D4	Biolegend	356930	B242459	2.5
CD4	PE-Dazzle594	YG610/20	RPA-T4	Biolegend	300548	B245173	0.3
CD8	APC-Cy7	R780/60	SK1	Biolegend	344714	B240888	2.5
ICOS	PE-Cy7	YG780/60	C398.4A	Biolegend	313520	B155585	1
PD1	PerCP-Cy5	B695/40	EH12.2H7	Biolegend	329913	B238928	1.25
CD25	BV650	V660/20	BC96	Biolegend	302633	B227756	1.25
Intracellular:							
Granzyme B	Pacific Blue	V450/50	GB11	Biolegend	515407	B220715	5
IL-17A	BV711	V710/50	BL168	Biolegend	512328	B241946	5
INFg	BV785	V780/60	4S.B3	Biolegend	502542	B226924	5
IL-21	AF647	R670/14	3A3-N2	Biolegend	513006	B176680	2.5
Foxp3	PE	YG582/15	150D	Biolegend	320008	B246346	5

Antibodies for flowcytometry staining for murine samples

Antigen	Fluorochrome	Filter	Clone	Company	Cat. Numb	Batch	Working dilution (ul)
Surface:							
CD45	PerCp/Cy55	B695/40	30-F11	BioLegend	103131	B205158	0.12
B220	APC-Cy7	R780/60	RA3-6B2	BioLegend	103223	B202710	0.6
NK1.1	APC-Cy7	R780/60	PK136	BioLegend	108723	B197398	1
Gr1	APC-Cy7	R780/60	RB6-8C5	BioLegend	108423	B203034	0.2
F480	APC-Cy7	R780/60	BM8	BioLegend	123117	B202743	0.6
PD-1	BV785	V780/60	29F.1A12	Biolegend	135225	B210953	0.12
CXCR5	BV650	V660/20	L138D7	Biolegend	145517	B207123	2
CD25	BV605	V610/20	PC61	Biolegend	102035	B195571	0.6
CD4	PE/Cy7	YG780/60	GK1.5	Biolegend	100421	B196263	0.25
CD127	Pe-CF594	YG610/20	A7R34	Biolegend	135031	B204489	0.25
Intracellular:							
IL-17A	Alx488	B530/ 30	TC11-18H10.1	Biolegend	506909	B193887	0.25
IL-21	Alx647	R670/14	BL25168	Biolegend	516803	B201762	0.06
IFNg	PE	YG582/15	XMG1.2	Biolegend	505807	B194985	0.12

Validation

We validated the antibodies following a two-step approach to ensure specificity and optimal performance. First, we adhered closely to the manufacturer's guidelines regarding recommended dilutions and storage conditions. In addition, prior to conducting the actual experiments, we performed preliminary optimization assays to determine the most effective antibody dilutions under our specific experimental conditions. This included titration series and assessment of signal specificity and background. These steps allowed us to confidently proceed with the experiments using validated working concentrations.

Animals and other research organisms

Policy information about studies involving animals; ARRIVE guidelines recommended for reporting animal research, and Sex and Gender in Research

Laboratory animals	C57BL/6 mice (Charles River, UK) and Slc5a12 KO mice (produced by the Sanger Institute via CRISPR/Cas9). 10-13 week-old.
Wild animals	The study did not involve wild animals.
Reporting on sex	Yes, we are reporting the sex of the animals used in our study. For this research, we exclusively used male mice. The decision to use only male mice was based on minimizing biological variability introduced by hormonal fluctuations in females, which can affect immune responses and metabolic pathways relevant to this study. This approach ensured greater consistency and reproducibility in the experimental data.
Field-collected samples	Mice were housed in a controlled environment with a 12-hour light/dark cycle, with lights on at 7:00 a.m. and off at 7:00 p.m. They had ad libitum access to food and water and were kept at a constant temperature of 22 ± 2°C and humidity of 50 ± 10%.
Ethics oversight	The study was approved by the institutional Animal Welfare and Ethical Review Body (AWERB) and conducted in accordance with national and international guidelines for the care and use of laboratory animals. All experimental protocols were reviewed and approved to ensure adherence to ethical standards aimed at minimizing harm and distress to the animals. Animal housing, handling, and experimental procedures complied with the guidelines established under the Animal (Scientific Procedures) Act 1986 in the UK. Every effort was made to ensure the highest standards of welfare throughout the study.

Note that full information on the approval of the study protocol must also be provided in the manuscript.

Clinical data

Policy information about clinical studies

All manuscripts should comply with the ICMJE guidelines for publication of clinical research and a completed CONSORT checklist must be included with all submissions.

Clinical trial registration	TRACTISS (ISRCTN: 65360827, EudraCT Number: 2010-021430-64
Study protocol	The TRACTISS protocol: a randomised double blind placebo controlled clinical trial of anti-B-cell therapy in patients with primary Sjögren's Syndrome. Brown S, Navarro Coy N, Pitzalis C, Emery P, Pavitt S, Gray J, Hulme C, Hall F, Busch R, Smith P, Dawson L, Bombardieri M, Wan-Fai N, Pease C, Price E, Sutcliffe N, Woods C, Ruddock S, Everett C, Reynolds C, Skinner E, Poveda-Gallego A, Rout J, Macleod I, Rauz S, Bowman S; TRACTISS trial team. BMC Musculoskelet Disord. 2014 Jan 17;15:21. doi: 10.1186/1471-2474-15-21
Data collection	Clinical data were collected between August 2011and January 2014
Outcomes	TRACTISS results were reported in full in "Randomized Controlled Trial of Rituximab and Cost-Effectiveness Analysis in Treating Fatigue and Oral Dryness in Primary Sjogren's Syndrome. Bowman SJ, Everett CC, O'Dwyer JL, Emery P, Pitzalis C, Ng WF, Pease CT, Price EJ, Sutcliffe N, Gendi NST, Hall FC, Ruddock SP, Fernandez C, Reynolds C, Hulme CT, Davies KA, Edwards CJ, Lanyon PC, Moots RJ, Roussou E, Giles IP, Sharples LD, Bombardieri M. Arthritis Rheumatol. 2017 Jul;69(7):1440-1450. doi: 10.1002/art.40093. Epub 2017 Jun 5"

Plants

Seed stocks	N/A
Novel plant genotypes	N/A
Authentication	N/A

Flow Cytometry

Plots

Confirm that:

☒ The axis labels state the marker and fluorochrome used (e.g. CD4-FITC).

☒ The axis scales are clearly visible. Include numbers along axes only for bottom left plot of group (a 'group' is an analysis of identical markers).

☒ All plots are contour plots with outliers or pseudocolor plots.

☒ A numerical value for number of cells or percentage (with statistics) is provided.

Methodology

Sample preparation	Mononuclear cell suspensions were obtained from whole blood and salivary gland biopsies (lip and parotid) of patients with Sjögren's disease. Blood samples were processed using density gradient separation, while biopsies were placed in culture medium to allow spontaneous egression (24h) of cells. For murine salivary glands samples, four hours prior to surgery, mice were injected via the tail vein with 100 µL of 2.5 mg/mL Brefeldin A (resuspended in PBS) to enhance intracellular cytokine staining. Murine salivary glands were collected and enzymatically digested in medium containing collagenase D (Roche) and DNase I (Sigma-Aldrich) for 15 minutes at 37°C to obtain a single-cell suspension.
Instrument	LSR Fortessa II (BD Biosciences) flow cytometer
Software	FlowJo V.10 software
Cell population abundance	N/A
Gating strategy	For human experiments, events were gated on viable cells, while murine samples were gated for viable/CD45+ cells. Where relevant, a dump channel was used to exclude nonrelevant populations (human panels V510/20, murine panels R780/60). Fluorescence minus one (FMO) controls were included to enable compensation and precise gating, respectively.

☒ Tick this box to confirm that a figure exemplifying the gating strategy is provided in the Supplementary Information.